Univerzita Karlova v Praze
Matematicko-fyzikální fakulta

Diplomová práce

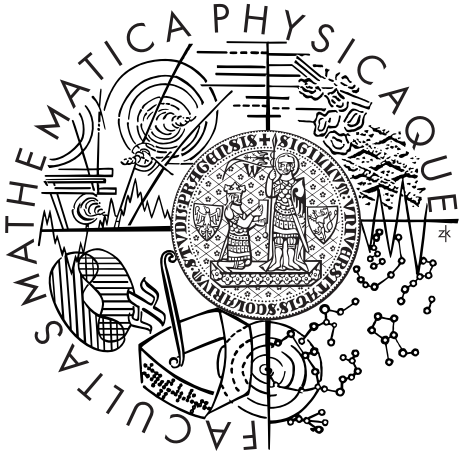

Bc. Estera Štefániková

Experimentální studium centrální a okrajové oblasti prstence plazmatu na tokamaku Compass

Katedra fyziky povrchů a plazmatu

Vedoucí diplomové práce: prof. RNDr. Milan Tichý, DrSc.

Studijní program: Fyzika

Studijní obor: Fyzika povrchů a ionizovaných prostředí

Praha 2014

Charles University in Prague
Faculty of Mathematics and Physics

MASTER THESIS

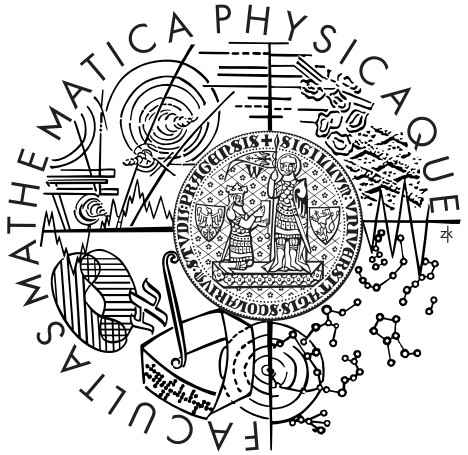

Bc. Estera Štefániková

Experimental study of central and edge regions of plasma column on Compass tokamak

Department of Surface and Plasma Science

Supervisor of the master thesis: prof. RNDr. Milan Tichý, DrSc.

Study programme: Physics

Specialization: Physics of Surfaces and Ionized Media

Prague 2014

Moje veľké poďakovanie patrí predovšetkým:
vedúcim tejto práce, prof. RNDr. Milanovi Tichému, DrSc. a RNDr. Petre Bílkovej, PhD. za starostlivé vedenie, cenné rady a prívetivý prístup;
celému COMPASS tímu za podnetné a príjemné pracovné prostredie;
TS tímu - mojej "druhej rodine";
a v neposlednom rade skutočnej rodine a priateľom za oporu.

I declare that I carried out this master thesis independently, and only with the cited sources, literature and other professional sources.

I understand that my work relates to the rights and obligations under the Act No. 121/2000 Coll., the Copyright Act, as amended, in particular the fact that the Charles University in Prague has the right to conclude a license agreement on the use of this work as a school work pursuant to Section 60 paragraph 1 of the Copyright Act.

In Prague date ..... signature

Název práce: Experimentální studium centrální a okrajové oblasti prstence plazmatu na tokamaku Compass

Autor: Bc. Estera Štefániková

Katedra: Katedra fyziky povrchů a plazmatu

Vedoucí diplomové práce: prof. RNDr. Milan Tichý DrSc., Katedra fyziky povrchů a plazmatu

Abstrakt: Diagnostika Thomsonova rozptylu s vysokým rozlišením na tokamaku COMPASS měří radiální profily elektronové teploty a hustoty v centrální a okrajové části plazmatu. Prostorové rozlišení v okrajové části je optimalizováno na studium okrajové transportní bariéry, která se formuje během módu s vyšším udržením (tzv. H-mod). Jsou pozorovány charakteristické krajové profily s tzv. pedestalem, o který se středový profil teploty a hustoty zvýší. Tvar pedestalu lze popsat funkcí modifikový hyperbolický tangens, což je pětiparametrový model, kterým se získají důležité parametry pedestalu jako např. výška a šírka. Nově je v této práci ukázáno fitování celých radiálních profilů elektronové teploty, hustoty a tlaku s pedestalem. Fitování se dál využije ve statistickém zpracování hodnot teploty a hustoty na vrcholu pedestalu, kdy chceme najít hranici tlaku oddělující režim H-modu.

Klíčová slova: diagnostika vysokoteplotního plazmatu, Thomsonov rozptyl, H-mod, transportní bariéra, parametre plazmatu

Title: Experimental study of central and edge regions of plasma column on Compass tokamak

Author: Bc. Estera Štefániková

Department: Department of Surface and Plasma Science

Supervisor of the master thesis: prof. RNDr. Milan Tichý DrSc., Department of Surface and Plasma Science

Abstract: High-resolution Thomson scattering system on the COMPASS tokamak provides electron temperature and density profiles in the central and edge plasma region. The spatial resolution in the edge plasma region is optimized for edge transport barrier studies. Formation of characteristic edge profiles (pedestals) is observed during high-confinement mode, i.e. the core electron temperature and density are raised up by the value of pedestal height. Both the electron and density pedestals are well-fitted by a modified hyperbolic tangent (mtanh) function, a five parameter model giving important parameters such as pedestal height and width, necessary for further analysis of the physics behind the transport barrier formation. A fitting technique of the full radial profiles of electron temperature, density and pressure during H-mode is also described. Using the fitting, electron temperature and density on top of pedestal are statistically processed to find a possible threshold for various H-mode regimes.

Keywords: high-temperature plasma diagnostics, Thomson scattering, H-mode, transport barrier, plasma parameters

Contents

Introduction

Research of controlled thermonuclear fusion aims at realizing an environmentally acceptable and almost unlimited energy source for future generations. It is generally accepted that the tokamak is the most promising device to confine fusion-relevant plasma using strong magnetic field. The largest experimental tokamak-type device ITER is currently being built in Cadarache, France. Its aim is to demonstrate the safe energy production with fusion power of 500 MW, to optimize the operational scenarios and to test the technologies that will be later used in the first demonstrative fusion power plant, the DEMO.

A future fusion power plant needs a quasi-stationary high-temperature plasma confined inside a vacuum-vessel with a first wall surviving extremely high heat fluxes. It was discovered that the required efficiency can be reached only if the tokamak operates in the regime with a high confinement, called H-mode.

Particular problems of ITER relevant physics are also studied in the Institute of Plasma Physics, AS CR, in Prague at the COMPASS tokamak, which has been relocated from the Culham Laboratory in the United Kingdom in 2007. The COMPASS tokamak is in operation from 2009. It is a medium-size tokamak with a clear H-mode and ITER-like geometry, which enables to investigate the physical processes during the tokamak operation and then scale the results. One of the most important parts of the research is investigation of the edge plasma region with external transport barriers that is formed during the high-performance operation.

One of the aims of this thesis is to contribute to a better understanding of these edge transport barriers, as they are also related to instabilities causing the transport barrier to collapse and leading to a lower plasma confinement. The key plasma parameters describing the transport barrier region, the electron temperature and electron density, will be measured by high-resoulution Thomson scattering diagnostic system at the COMPASS tokamak.

1. Magnetic confinement fusion

1.1 Nuclear fusion

Nuclear fusion has a potectial to be the main energy source for future generations. On one hand, the Earth has plenty of raw materials for fusion reaction (deuterium, lithium), pruducts have short radioactive half-life, and fusion reactors do not have likely meltdown scenarios. On the other hand, mankind has never been able to control fusion reaction with positive energy balance yet. Conditions to ignite and maintain fusion reaction are pushing our technology limits since the middle of the last century.

Fusion energy is produced, if two or more light nuclei fuse into heavier ones whose mass is smaller then the total mass of the reactants. The released energy can be calculated from the famous Einstein formula $E = mc^2$, where m is the mass difference. The favored fusion reaction is the so-called "DT" reaction

$$ {}^3_1T + {}^2_1D \rightarrow {}^4_2He + {}^1_0n + 17.6\,\mathrm{MeV}, \tag{1.1} $$

thanks to its highest cross-section at the lowest temperature (figure 1.1).

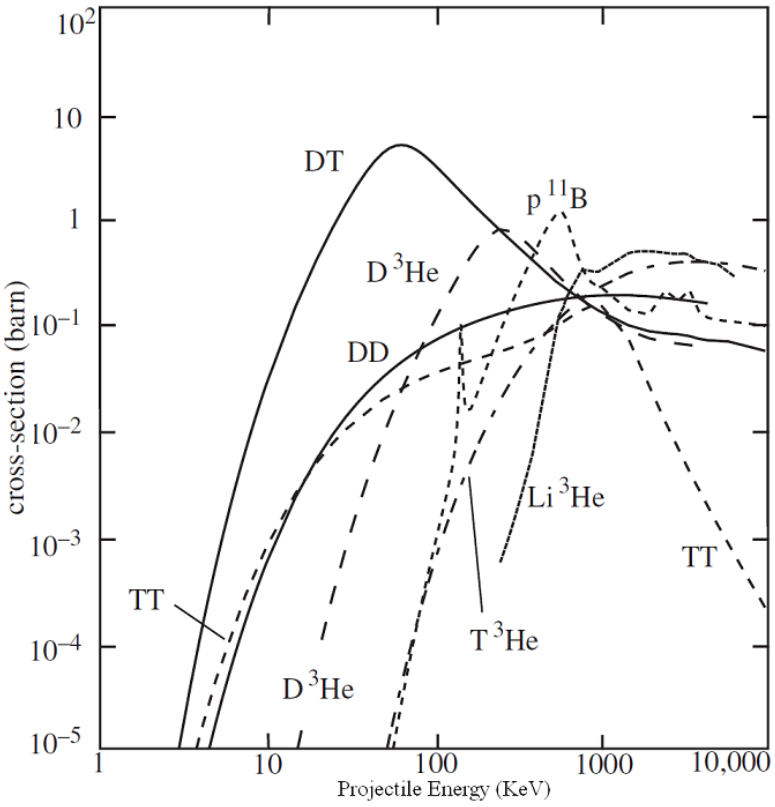

Figure 1.1: Cross-sections of several fusion reactions [1]. 1 KeV $\approx 10^7$ degrees.

The fusion energy is released as the kinetic energy of the reaction products. The helium ion is four times heavier then the neutron, and therefore it receives only 20% of the energy; this energy is provided to plasma as the hot ion collides many times before it escapes. On the contrary, the neutron leaves the plasma

almost immediately, and delivers its 80% of the fusion energy to the materials of the reactor's first wall, from where it is extracted by the cooling system.

1.2 Tokamaks

On figure 1.1 it can be seen that the temperature relevant for fusion is around 200 million degrees. One of the approaches to achievement of such temperature is to magnetically confine hot plasma inside a vacuum chamber, preventing its particles from reaching the wall and cooling down.

The most promising, and widely used, magnetic confinement fusion device is a tokamak, whose name is an acronym of russian words *toroidal'naya kamera s magnitnymi katushkami* (toroidal chamber with magnetic coils). The history of tokamak devices has begun in the Kurchatov Institute in 1956, in the research led by Lev Artsimovich. Tokamak holds charged particles by means of a strong magnetic field which has a complex helical shape (figure 1.2); its toroidal component (blue arrow in the figure) is created by a set of external coils, while its poloidal component (green arrows) is created by the toroidal current flowing through plasma. According to the original design, this current is induced by the time derivative of the current in inner poloidal field coils through the transformer effect, which is however not suitable for a steady state tokamak operation, as only a DC plasma current provides a stable magnetic configuration. Therefore, several additional current-drive mechanisms, using microwave or neutral particle beams, have been introduced.

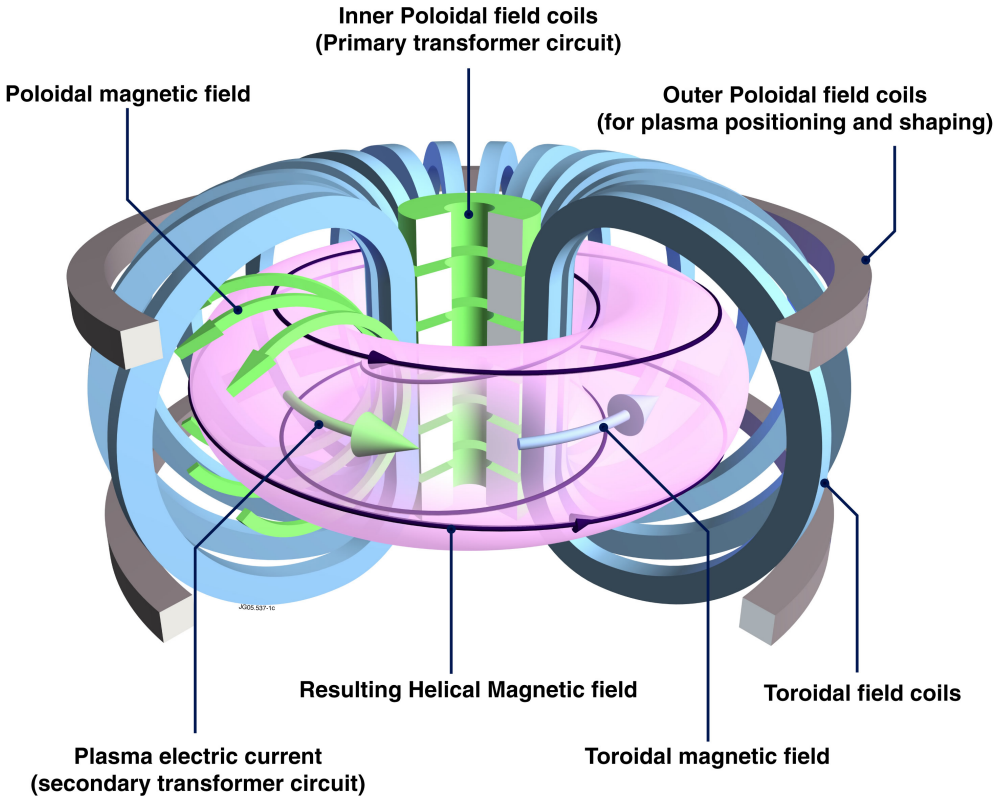

Figure 1.2: Schematic picture of tokamak. Image: EFDA-JET [2].

1.3 The COMPASS tokamak

The COMPASS (COMPact ASSembly) tokamak is a medium-sized tokamak (see table 1.1 with parameters) and it is one of the three European tokamaks (JET, ASDEX-U and COMPASS) with ability to hold a plasma within advanced confinement mode (high confinement mode, usually refered to as 'H-mode') and with ITER-relevant geometry. COMPASS is the smallest from the group and thus very flexible to new experiments. Scientific program includes edge plasma studies, investigation of L-H transition (the transition between low-confinement and high-confinement mode), studies of plasma turbulence and particle transport.

Parameters	**Max. expected values**
Major radius R	0.56 m
Minor radius a	0.23 m
Plasma current Ip (max)	350 kA
Magnetic field BT	2.1 T
Vacuum pressure	2×10^{-6} Pa
Elongation	1.8
Plasma shape	SND, SNT, elliptical, circular
Pulse length(max)	1 s
Beam heating PNBI 40 keV	2 x 0.3 MW

Table 1.1: The COMPASS tokamak characteristics.

1.4 H-mode

The high-confinement regime (H-mode) is planned as a standard operating regime for the future nuclear fusion power plant, as it spontaneously increases the stored energy in the plasma compared to L-mode. H-mode was observed for the first time on tokamak ASDEX by Wagner et al. [3]. Since then other tokamaks including COMPASS frequently study this regime. It requires a specific plasma configuration and a heating power above a certain threshold. H-mode can be characterised by a sudden drop in D_α radiation and with a spontaneous steeping of the edge density gradient due to the locally reduced transport at the edge of plasma, which is also called the edge transport barrier. Other signatures are an increase of the average density, rise in the stored energy and confinement of energy and particles. Certain edge instabilities, such as the edge localized modes (ELMs) are connected to this regime, which release the particles from plasma, leading to loss of confinement. Various techniques of ELMs mitigation/suppression are therefore being investigated.

1.5 EFIT

The EFIT (Equilibrium FITting) code is one of the codes used for equilibrium reconstruction. Currently used version is EFIT++, written in C++ with computation core in Fortran 95. From this reconstruction we obtain information about the tokamak magnetic configuration (poloidal magnetic flux ψ, magnetic

axis), current and pressure profiles, current profile parameters, information about plasma geometry (plasma shape, volume), safety factor and stored energy. As a fundamental inputs, data from magnetic sensors, plasma current, poloidal field coils geometry and currents, toroidal magnetic field and limiter geometry is taken. In order to obtain a good equilibrium, the currents in the passive structures (vacuum vessel, PF coils casings and short-circuited PF coils) also have to be included. There might be other possible additional inputs, such as pressure profile (from high-resolution Thomson scattering), integrated magnetic field (Faraday rotation), etc. The reconstruction is performed by numerical iterative solving of the Grad-Shafranov (GS) equation.

1.5.1 Grad-Shafranov equation

The GS equation is a two-dimensional, nonlinear, second order partial differential equation arising from ideal MHD theory that describes equilibrium of configurations possessing toroidal symmetry. We consider Maxwell equations:

$$div\vec{B} = 0 \tag{1.2}$$

$$rot\vec{B} = \mu_0\vec{j} \tag{1.3}$$

$$rot\vec{E} = 0, \tag{1.4}$$

where $\vec{B}$ is magnetic induction, μ_0 is magnetic permeability, $\vec{j}$ is current density and $\vec{E}$ is electric intensity; and MHD equation of motion:

$$\nabla p = \vec{j} \times \vec{B}, \tag{1.5}$$

where p is plasma pressure. In the cylindrical coordinates (R, φ, z), for the case of toroidal symmetry $\vec{B} = \vec{B}(R, z) \neq \vec{B}(\varphi)$, the equation (1.1) is satisfied by introduction of the poloidal flux function ψ:

$$\psi(R, z) = \frac{1}{2\pi} \int \vec{B}.d\vec{S}, \tag{1.6}$$

where $d\vec{S}$ is a surface element extending between constant pressure surfaces oriented in the poloidal direction. The relation $\psi(R, z) = const$ defines magnetic surfaces (also called flux surfaces) and they coincide with the constant pressure surfaces. Let

$$F(\psi) = RB_\phi, \tag{1.7}$$

where the magnetic field written in terms of a flux function $\psi(R, z)$ is

$$\vec{B} = \nabla\psi \times \frac{\vec{e_\phi}}{R} + B_\phi(R, z)\vec{e_\phi}. \tag{1.8}$$

Then together with the definition of poloidal flux function ψ, Maxwell equations (1.1)-(1.3), and MHD equation of motion (1.4), the GS equation can be derived [4]:

$$R^2\nabla.\left(\frac{\nabla\psi}{R^2}\right) = -\mu_0 R^2 \left(\frac{dp}{d\psi}\right) - F\left(\frac{dF}{d\psi}\right). \tag{1.9}$$

Given the functions $p(\psi)$ and $F(\psi)$, along with the appropriate boundary conditions, the GS equation can be solved for $\psi(R, z)$. This gives the equilibrium flux distribution. However, the functions p and F are nonlinear in general and there might be no solution, or more solutions satysfying both the GS equation and the boundary conditions.

EFIT solves the GS equation modified with additional terms - current densities in PF coils (experimentally measured) and in passive structures (current profile in the vacuum vessel is not measured, it has to be provided by induced currents model). Then the undetermined linearized set of equations is solved by iterative least square method of the computed and measured values using single value decomposition method.

1.5.2 Remapping of the plasma parameters along magnetic surfaces

As mentioned above, the equilibrium reconstruction output is distribution of the poloidal flux ψ, which is constant on magnetic surfaces. It is convenient to introduce normalized flux ψ_n. It "numberes" the magnetic surfaces, as it is equal to 0 on magnetic axis and to 1 on the last closed flux surface (LCFS). Experimental data, e.g. the profiles of electron temeperature and density from high-resolution Thomson scattering which are originally measured along the vertical coordinate z, are often depicted in ψ_n as it is relevant for various devices. Another often used possibility is to remap the data that are not measured along the midplane (plane where $z = 0$) to the coordinate R using the assumption, that plasma parameters are constant along magnetic surfaces. This remapping is a part of program 'EFIT 2D mapping' written by V.Weinzettl.

2. Introduction to Thomson scattering theory for high temperature fusion plasmas

2.1 Thomson scattering

Thomson scattering (TS) is a laser-aided plasma diagnostics. It is based on scattering of electromagnetic waves by free electrons. This process was first described by J.J. Thomson in 1906 [5]. A brief overview on TS as a diagnostic tool is given in [6]. The experimental application of TS was coupled with development of high-power light sources. In 1963, Fiocco et al. [7] and Funfer et al. [8] first demonstrated the incoherent TS as a diagnostic tool for laboratory plasmas, where a few photons were observed per scattering event. The role of TS as a diagnostics suitable for high-temperature plasmas was established in 1969, when Peacock et al. [9] measured the electron temperature in the Russian T-3 tokamak. A development of TS diagnostic systems continues to present, where modern systems are able to detect over 1000 photons for a single scattering event in plasma. They are used as a standard tool for measurements of the electron temperature and density of hot magnetically confined plasmas with high spatial and time resolution along the plasma diameter.

When a monochromatic electromagnetic radiation is fired into high-temperature plasma, it is scattered by electrons. The oscillating electric field of the incident wave causes an electron to oscillate at the same frequency. The oscillating electron then emits radiation concentrated in direction perpendicular to its oscillation. The emitted radiation has a dipole pattern. The resultant spectrum is broadened due to the doppler effect (fig. 2.1).

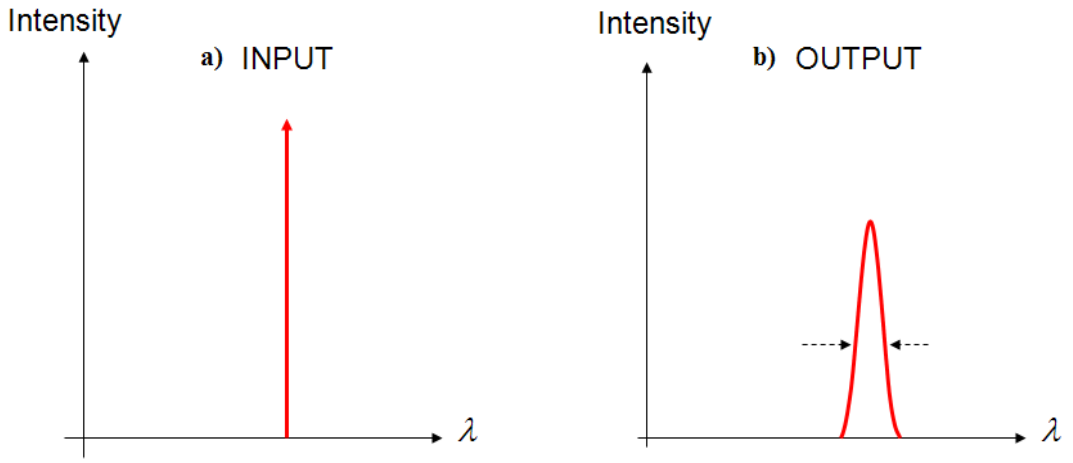

Figure 2.1: Schematic spectral broadening of incident monochromatic laser radiation (a) after scattering on free hot electrons in plasma due to the doppler effect (b).

The character of the scattering process depends not only on the number of electrons, but also on the interactions between them [6]. The parameter that helps to distinguish whether the collective electron phenomena influence the process of scattering or not, is called the Salpeter scattering parameter α [10]

$$\alpha = \frac{1}{k\lambda_D} = \frac{\lambda_0}{4\pi\lambda_D sin\frac{\theta}{2}}, \tag{2.1}$$

where λ_0 is the wavelength of the incident electromagnetic wave, λ_D is the Debye length, and θ refers to the angle between the incident wave and scattered wave directions. Depending on the value of α, three cases can be distinguished:

1. $\alpha << 1$
   When the incident wavelength is much smaller than the Debye length, the total scattered power is obtained as an incoherent summation over the scattered powers of the individual electrons. The scattering spectrum is therefore determined by the electron velocity distribution, from which the local values of electron temperature and density can be derived. This type of scattering process is called incoherent TS and it will be the subject of this thesis.

2. $\alpha \geq 1$
   In this case, the scattering contributions from electrons and their surrounding shielding "cloud" will add up coherently, since they have a negligible phase difference. The ions are usually surrounded by a shield that consists of approximately one half of electrons and the other half consists of ions [6]. It is the scattering by the electrons in this shield that can be observed experimentally. It is called coherent scattering, or also ion scattering, because the information about the ion velocity distribution can be gained from this process. In 1983, there was an attempt to use the coherent scattering to measure the ion temperature at Alcator-C tokamak. It is experimentally a very challenging technique and has been applied at a very few devices.

3. $\alpha \sim$ 5-20
   When the Salpeter parameter is much larger than 1, the scattered power is proportional to the to the square of the density fluctuation level and collective motion of electrons can be observed. It is called collective scattering and it can be used to measure the electron fluctuation spectrum in the plasma.

In this thesis, we will further investigate only the incoherent scattering case, as it is used as a basic set-up for experimental measurements of the electron temperature and density profiles on most of the current fusion devices, including the COMPASS tokamak.

2.1.1 Thomson scattering spectrum

The complete description of theory of the incoherent Thomson scattering for high-temperature fusion plasmas involves complex electrodynamics with complicated mathematical framework; therefore it is not the aim of this thesis. However, when the electron temperature reaches several keV, the relativistic treatment of the electron motion is necessary when analyzing scattered data, as the equation of motion of the electron and the electron velocity distribution function are modified. This is particularly important for bigger fusion devices like ITER, where high order relativistic effects dramatically affect the TS spectrum. Their impact on the spectrum starts to be visible at the temperature of 1 keV, which is measured also at the COMPASS tokamak. Therefore the most important effects will be described with emphasis on rather intuitive understanding of their influence on the TS spectrum.

2.2 Thomson scattering theory

The problematics of Thomson scattering was already described in many sources. Probably the most complex and comprehensive work on this topic was done by S. L. Prunty in his (yet) unpublished materials called "A primer on Thomson scattering theory for high-temperature fusion plasmas". This thesis follows the theory explanation presented in [11], [12] and [14].

2.2.1 The electron velocity distribution

To derive the TS spectrum, it is necessary to start with the electron velocity distribution. For and ideal gas with particle velocity v, mass m and temperature T, the Maxwell-Boltzmann distribution is given by:

$$f(v)d^3v = \left(\frac{m}{2\pi kT}\right)^{\frac{3}{2}} \exp\left(\frac{-\frac{1}{2}mv^2}{kT}\right) 4\pi v^2 dv. \tag{2.2}$$

Velocity of free electrons in high-temperature plasma is of significant proportion of the speed of light c, therefore the relativistic electron velocity distribution has to be considered:

$$f(\beta) = \frac{\alpha}{2\pi K_2(2\alpha)} \frac{exp\left[-2\alpha(1-\beta^2)^{-\frac{1}{2}}\right]}{(1-\beta^2)^{\frac{5}{2}}}, \tag{2.3}$$

where

$$\beta = \frac{v}{c}, \tag{2.4}$$

$$\alpha = \frac{m_0 c^2}{2kT} \tag{2.5}$$

for an electron with rest mass m_0, related to the non-relativistic mass by relation $m = m_0\gamma$; γ is the Lorentz factor:

$$\gamma = \frac{1}{\sqrt{1-\beta^2}} \tag{2.6}$$

and

$$K_2(2\alpha) \cong \left(\frac{\pi}{4\alpha}\right)^{\frac{1}{2}} \exp(-2\alpha) \tag{2.7}$$

is a modified Bessel function of the second kind and of second order.

2.2.2 Acceleration of an electron by electromagnetic wave

When the electron is under the influence of the electric and magnetic field of an incident laser (E_i, B_i), the rate of change of the (relativistic) momentum is equal to the Lorentz force:

$$\frac{d}{dt}\frac{m_0\vec{v}}{(1-\vec{\beta}^2)^{\frac{1}{2}}} = -e(\vec{E_i} + \vec{v} \times \vec{B_i}), \tag{2.8}$$

where e is the electron charge. With $\beta = \frac{\vec{v}}{c}$, the above equation becomes:

$$m_0 c \frac{d}{dt} \frac{\vec{\beta}}{(1-\vec{\beta}^2)^{\frac{1}{2}}} = -e(\vec{E}_i + \vec{v} \times \vec{B}_i). \tag{2.9}$$

Following the derivation in [prunty], we finally obtain:

$$\frac{d\vec{\beta}}{dt} = -\frac{e}{m_0 c\gamma} \left(\vec{E}_i - (\vec{\beta}.\vec{E}_i)\vec{\beta} + \vec{v} \times \vec{B}_i \right), \tag{2.10}$$

which is the equation for the acceleration of an electron by an incident electromagnetic wave.

2.2.3 Scattered electric field

As shown in [11], the fundamental equation that relates the scattered electric field to the acceleration of the electron may be derived from the Lienard-Wiechert potentials:

$$\phi(\vec{r}, t) = \frac{q}{4\pi\epsilon_0} \left[\frac{1}{R - \vec{R}.\vec{\beta}} \right]_{ret} \tag{2.11}$$

is the scalar potential and

$$\vec{A}(\vec{r}, t) = \frac{\mu_0 q}{4\pi} \left[\frac{\vec{v}}{R - \vec{R}.\vec{\beta}} \right]_{ret} \tag{2.12}$$

is the vector potential, where q is a particle charge, ϵ_0 is permitivity, μ_0 is permitivity, $\vec{R} = \vec{r} - \vec{r}_e$ is a vector between the position of the observer $\vec{r}$ and the position of electron $\vec{r}_e$.

The quantities within square brackets were evaluated at the retarded time:

$$ret = t^{'} = t - \frac{|\vec{r} - \vec{r}_e(t^{'})|}{c} \tag{2.13}$$

that is taking into account the delay between the time of light emission and time of detection due to light travelling at relativistic velocities. The electric and magnetic fields are determined from:

$$\vec{E}(\vec{r}, t) = -\vec{\nabla}\phi(\vec{r}, t) - \frac{\partial \vec{A}(\vec{r}, t)}{\partial t}, \tag{2.14}$$

$$\vec{B}(\vec{r}, t) = -\vec{\nabla} \times \vec{A}(\vec{r}, t). \tag{2.15}$$

However, the scalar and the vector potentials are given in terms of the retarded position and time and therefore the vector operations have to be transformed. The resulting relation for the scattered (or radiated) electric field is [rory diz]:

$$\vec{E}_s(\vec{r}, t) = \left[\frac{e}{c^2 R} \frac{\hat{s} \times (\hat{s} - \vec{\beta}) \times \dot{\vec{\beta}}}{(1 - \hat{s}.\vec{\beta})^3} \right]_{ret}. \tag{2.16}$$

where $\hat{s}$ is a unit scattering vector towards the observer. The term $(1-\hat{s}.\vec{\beta})^3$ comes from the evaluation of the vector and scalar potentials at the retarded time and is of great importance because of determining the shape of the scattered spectrum.

2.2.4 Scattered power and scattering cross-section

The power scattered into some solid angle $\Delta\Omega$ at some frequency $\omega_s^* = \omega_i \left(\frac{1-\vec{\beta}.\hat{s}}{1-\vec{\beta}.\hat{i}}\right)$, where $\hat{i}$ is a unit incident vector, is related to the square of the scattered electric field E_s as [rory diz]:

$$P_s(\omega_s) = c\epsilon_0 r_{el}^2 \Delta\Omega E_s^2 \delta(\omega_s - \omega_s^*), \tag{2.17}$$

where r_{el} is the classical electron radius and δ represents the Dirac delta function. After substituing from the previous equations and ignoring the scalar quantites, on the rhs we obtain [12]:

$$\hat{s} \times (\hat{s} - \vec{\beta}) \times (\vec{E}_i - (\vec{\beta}.\vec{E}_i)\vec{\beta} + \vec{v} \times \vec{\beta}_i), \tag{2.18}$$

where $\vec{E}_i$ means incident electric field vector. Using vector identities, this term can be divided into three parts showing how the relativistic depolarisation effect and the blue shift originate from the three components of electron acceleration $\dot{\vec{\beta}}$ and their interaction [12].

In [12], the scattered electric field magnitude and polarisation due to each of the three components of electron acceleration are calculated. By substituing the resulting expressions into the equation for scattered electric field $\vec{E}_s$ and into the equation for the scattered power $P_s(\omega_s)$, we finally obtain:

$$P_s(\omega_s) = \frac{c\epsilon_0 r_{el}^2 \Delta\Omega}{\gamma^2} \frac{E_i^2}{(1-\vec{\beta}.\hat{s})^2} \frac{(1-\vec{\beta}.\hat{i})^2}{(1-\vec{\beta}.\hat{s})^2} \left[1 - \frac{(\vec{\beta}.\vec{E}_i)^2(1-cos\theta)}{(1-\vec{\beta}.\hat{s})(1-\vec{\beta}.\hat{i})}\right]^2 \delta(\omega_s - \omega_s^*), \tag{2.19}$$

where θ is the scattering angle. This expression is analytically integrated in order to obtain an approximation to the TS spectrum.

The scattered power is related to the scattering cross section per unit solid angle σ_{sv} by equation

$$\sigma_{sv}(\omega_s) = \frac{P_s(\omega_s)}{S_i \Delta\Omega}, \tag{2.20}$$

where S_i is the Poynting vector

$$S_i = \frac{1}{c\mu_0} E_i^2, \tag{2.21}$$

from which the expression for σ_{sv} can be obtained:

$$\sigma_{sv}(\omega_s) = \frac{r_{el}^2}{\gamma^2} \frac{1}{(1-\vec{\beta}.\hat{s})^2} \frac{\omega_s^{*2}}{\omega_i^2} \left[1 - \frac{(\vec{\beta}.\vec{E}_i)^2(1-cos\theta)}{(1-\vec{\beta}.\hat{s})(1-\vec{\beta}.\hat{i})}\right]^2 \delta(\omega_s - \omega_s^*). \tag{2.22}$$

The expression

$$\frac{1}{(1-\vec{\beta}.\hat{s})^2} \frac{\omega_s^{*2}}{\omega_i^2} \tag{2.23}$$

describes the blue shift and the expression

$$\left[1 - \frac{(\vec{\beta}.\vec{E}_i)^2(1-cos\theta)}{(1-\vec{\beta}.\hat{s})(1-\vec{\beta}.\hat{i})}\right]^2 \tag{2.24}$$

describes polarisation.

2.2.5 Relativistic effects on the TS spectrum

For the electron temperature of several hundreds of eV, relativistic effects have to be taken into account. An exhaustive derivation of their influence on the TS spectrum can be found for example in [11] and [12]. The complete description of these effects is far beyond the scope of this thesis, therefore only a brief insight into their impact will be given on the simulated relativistic spectrum (fig.2.2)

Relativistic blue shift

The blue shift, i.e. shift of the spectrum to lower wavelengths with increasing temperature, is characteristic on the TS spectrum. The term $\left(\frac{\omega_s}{\omega_i}\right)^2$ amplifies higher frequencies and hence lower wavelengths. Similarly, the term $\frac{1}{(1-\vec{\beta}.\hat{s})^2}$ amplifies the scattered power when $\vec{\beta}.\vec{s} > 0$, that is when electrons are moving towards the observer. As electrons moving towards the observer produce a negative wavelength shift, then amplifying this second term also results in a blue shift of the spectrum. Since the electron rest mass is $\approx$ 500 keV. An electron with a temperature of 1keV will have a velocity $\beta \approx 0.045$, thus the power spectrum ($P_s \propto E_s^2$) will be modified by a factor of 1.3 for electrons moving towards an observer or 0.7 for electrons moving away from an observer. Even at a low electron temperature a significant blue shift may ocur.

Finite transit time

A first order relativistic effect, the finite transit time, causes that the time an electron moving towards the observer appears to spend in the scattering volume is shortened. This results in a small red shift on an already strongly blue-shifted spectrum.

Headlight effect

Charged particles moving at the speed close to the speed of light radiate predominantly in their direction of motion.

Depolarisation

The depolarisation term arises from the component of the electron velocity vector parallel to the electric field vector of the incident field. It has a small effect on the shape of the spectrum, but a large effect on the total number of scattered photons [13]. It influences evem moderate fusion temperatures ($>$ 5 keV). It causes a significant reduction of scattered power and hence it has to be taken into account when measuring the electron density. For example, for a LIDAR back scattering system with reactor temperatures of 20-30 keV, there will be a reduction in scattered power of 15-20% [12].

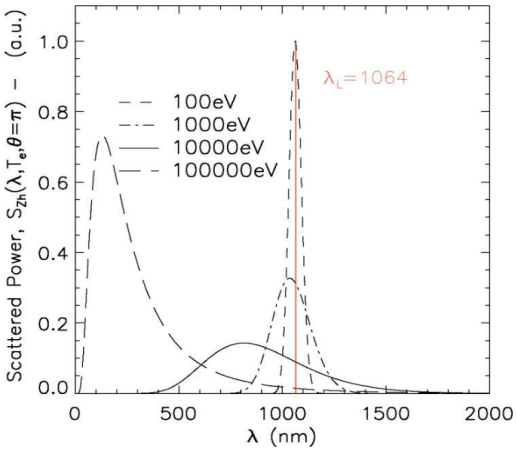

Figure 2.2: The Selden relativistic spectrum modified for the Naito depolarisation correction. The scattered power is described by the Selden function and is related to the number of scattered photons by a factor α. The spectrum is plotted for a range of T_e, constant but arbitrary n_e at a scattering angle of π [12].

3. Experimental set-up

3.1 The Nd:YAG Thomson scattering diagnostic system

3.1.1 Overview

The Nd:Yag Thomson scattering (TS) diagnostic system at COMPASS tokamak was designed to measure the electron temperature and density profiles in high-temperature plasmas throughout the plasma discharge. It consists of two parts that can work independently. The core TS system is collecting radiation in the region starting at 30 mm below the midplane (z=0), to 210 mm above the midplane with spatial resolution up to 7 mm; the edge TS system with spatial resolution uo to 3 mm was designed for the region from 200 mm to 300 mm above the midplane. Together, the TS system collects scattered radiation from 54 spatial points at the position R=0.557 m along vertical coordinate z, with an overlapping region in order to validate the connection between core and edge profiles. Schematically in the figure 3.1.

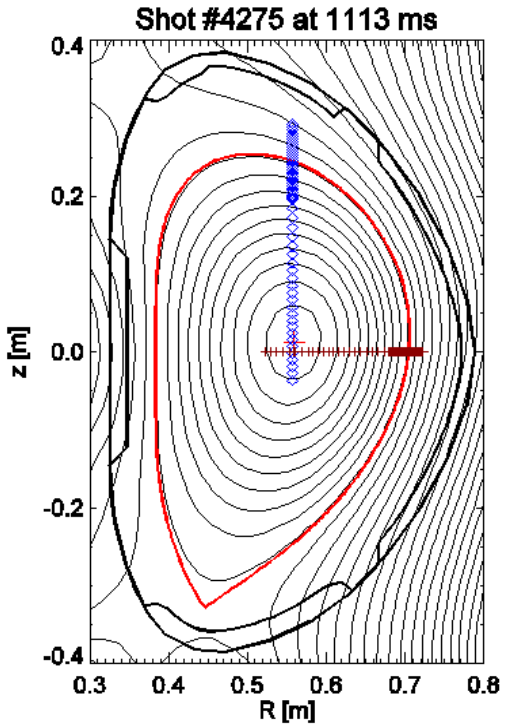

Figure 3.1: Poloidal cross-section of the tokamak vessel with reconstructed magnetic surfaces from EFIT at chosen time. The center of the plasma is not identical with center of the vessel. Red line depicts last closed flux surface. Blue points show 54 spatial points covered by TS diagnostics (at R=0.557 m). Dark red points show remapped TS points to midplane (z=0) along magnetic surfaces.

Thomson scattering diagnostics is an active spectroscopic method based on scattering of a monochromatic laser beam on free electrons in plasma; this phenomena is called incoherent scattering. The detected radiation is doppler shifted; the spectral broadening is proportional to the energy of the scattering electrons and therefore to the electron temperature, while the intensity of the scattered light is proportional to the electron density.

A scheme of experimental set-up of COMPASS TS diagnostic system is in the figure 3.2.

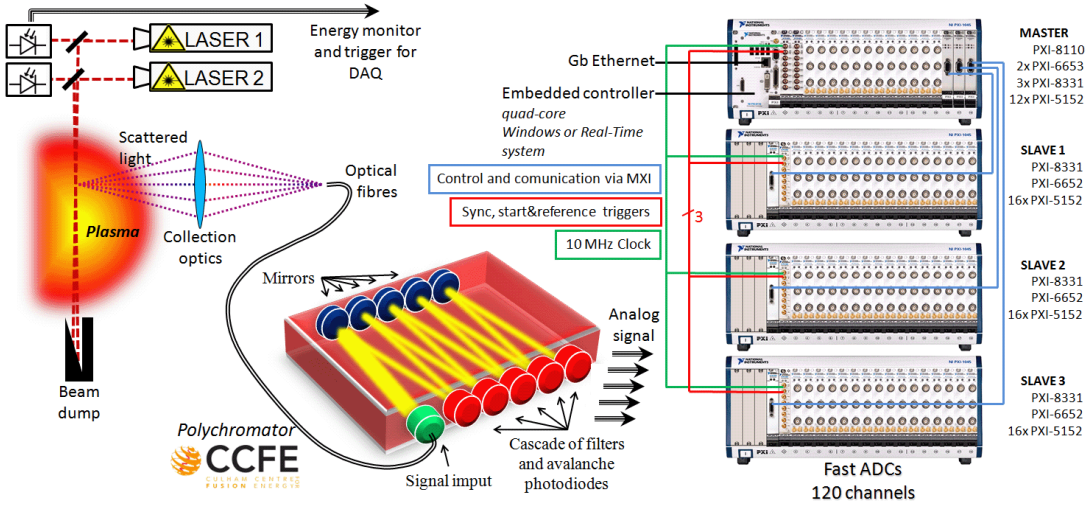

Figure 3.2: Schematic experimental set-up of the Thomson scattering diagnostics at COMPASS tokamak [courtesy Milan Aftanas].

As a high energy laser source, two Nd:YAG infrared lasers (wavelength of 1064 nm, energy of 1.5 J each during 7 ns pulse, repetition rate 30 Hz) were installed. Lasers can operate in three regimes: both lasers are fired simultaneously with total energy of 3 J and repetition rate 30 Hz; alternate mode - 1.5 J each, repetition rate 60 Hz; or "double pulse" mode with arbitrary pulse separation from 1 μs to 16.6 ms. Using double pulse regime would enable observation of fast events in the plasma like forming of the edge transport barrier called "pedestal" during H-mode, or measurement of the electron temperature and density profiles during edge localized modes (ELMs) instabilities.

Two objectives collect scattered radiation from the central and edge region of plasma under the angle around 90°. The objective for the core region consists of 5 elements. The f-number and magnification varies along the observed region; at the centre the values are f/5.9 and magnification of 0.34. Vertical resolution is 8.1-12.4 mm [14]. The edge region objective consists of 7 elements putting a higher demands on resolution and requiring off-axis field of view (scheme in the figure 3.3). At the center of the observed region it has f/6.05 and magnification of 0.35. The resolution starts at 3 mm and varies to 4.6 mm when moving outwards from the center.

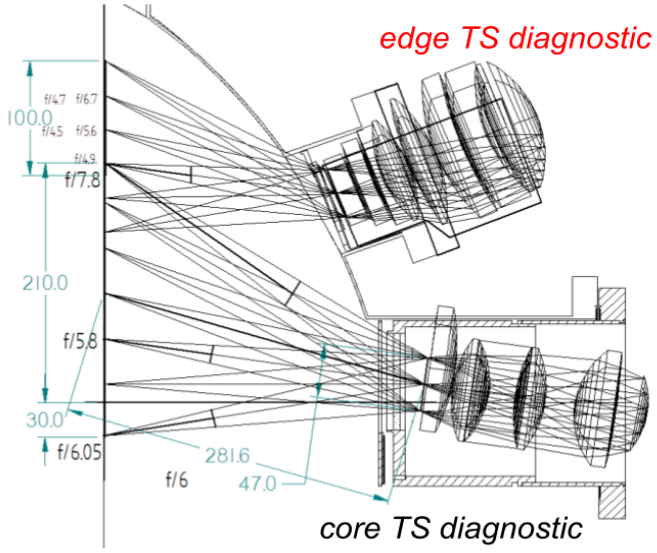

Figure 3.3: Design of the collection optics for TS system at the COMPASS tokamak [15].

Optical system focuses radiation in a bunch of optical fibres. The fibres are made of polymer cladding silica with core diameter of 210 μm and 230 μm cladding diameter. 12 fibre bunches are used for central region, 16 for core region and 1 extra bunch is used for position alignment. Configuration of fibre bundles is shown in the figure 3.4. The width of the fibre bundle covers the whole image of laser beam diameter with 1 mm tolerance for potential misalignment. The laser beam misalignment can be checked by split-fibre bundle. It has the same size as the other fibre bundles, but it is divided into two halves. From the ratio of signals in the halves, the direction of misalignment can be determined [14]. Figure 3.5 shows randomized circular end of the fibre bundle.

Optical fibres lead the signal into set of 29 filter polychromators with avalanche photodiode (APD) detectors that have a high sensitivity in the near infrared region. In principle, each spatial point requires an individual filter polychromator. The number of polychromators can be reduced using duplexing method, where the signal from two spatial points is led into one polychromator through the fibres of different lenght; the points are distinguish according to time delay of the signal. Length of the shorter arm is 20 m and, the longer arm has 33 m.

In each polychromator, there is a set of filters that divide incoming light into 5 spectral channels, which is then imagined onto the APD and converted to electric signal. Data from each polychromator and each spectral channel has to be digitized individually. Only four of five spectral channels are digitized according to expected electron temperature range at corresponding spatial point. The spectral filters were designed for the temperature range of 10 eV - 5 keV.

Signal from all 29 polychromators is digitized at the same time using a 120 channel 1GSample/s fast analogue digital converter (ADC) system with 8 bit resolution. ADC records the (fast) temporal evolution of measured signal on a slowly changing background and thus has the possibility to optimize its supression. This can be done using a 16 bit slow ADCs with sampling rate of 500 kSample/s.

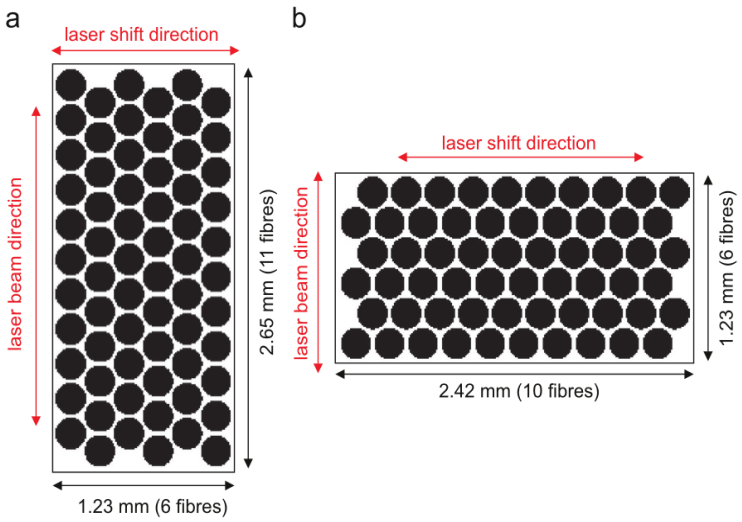

Figure 3.4: Configuration of the fibre bundles in (a) core TS system, (b) edge TS. In the core system, the fibres in bundles are arranged in hexagonal pattern in rectangle of 6 x 11 fibres, oriented with longer side along the image of the laser beam. In edge system, the fibres are arranged in rectangle of 10 x 6 with shorter side along the image of the laser beam. On the polychromator side, the fibres are arranged circularly with 3 mm diameter [16].

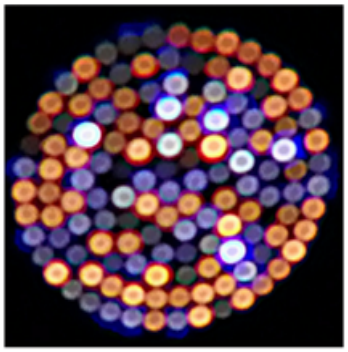

Figure 3.5: Randomized circular end of fiber bundle illuminated by light sources of different colors [17].

3.2 Signal processing

3.2.1 Calibration

To determine both electron temperature and density, relative spectral and absolute density calibrations of the system are necessary. The main source of non-uniformity in spectral transmission is the detector (APD) gain.

Spectral calibration

Spectral calibration is mandatory to reconstruct scattered spectrum shape. The scattered light is spectrally analyzed in 29 polychromators using a set of five spectral filters and APD detectors. Parameters of spectral filters (central wavelenght and bandwidth) have to be determined to enable measurement of electron temperature in the range of 10 eV to 5 keV [17]. A polychromator spectral calibration is performed using the set-up shown in the fig.3.6.

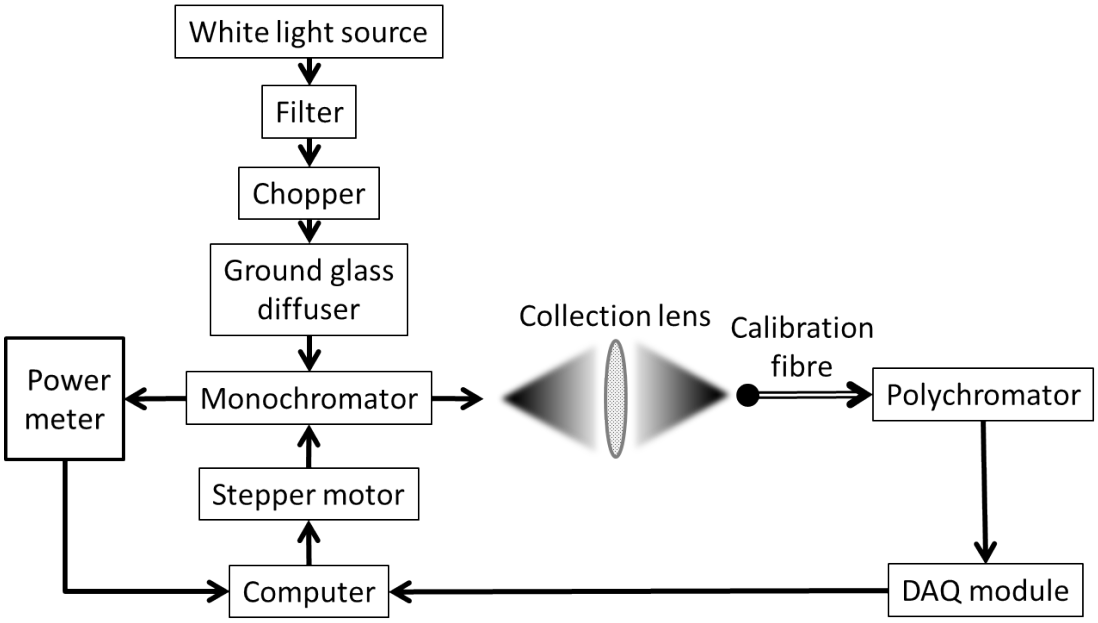

Figure 3.6: Schematic layout for spectral calibration [courtesy Milan Aftanas]

Halogen lamp (Oriel LSB116/5) is used as a source of continuous and stable white light. Light with wavelength lower than 610 nm is blocked by the filter to assure that higher order diffraction do not affect the calibration process. Light chopper is incorporated to the calibration scheme to provide additional precision with subtracting dark signal. Entrance slit of the monochromator (Newport Cornerstone 260, 1200 lines/mm grating model 77990) is illuminated uniformly by the means of ground glass diffuser. Light of the selected wavelength exit the monochromator with either axial or lateral slit. In our configuration, collection lens is placed after lateral exit slit to couple all available light to optical fibre. Optical fibre is the same design as fibres used for TS system, with length of 27.5 m, which is arithmetic mean of the duplexed bundles (20 m and 33 m). The optical fibre leads the light of the selected spectrum into the polychromator. A

thermoelectricaly cooled silicon photodetector (Oriel 71651) with calibration provided by manufacturer is attached to spectrometer axial output slit. This detector provides calibration of the white light source used for the spectral calibration.

The calibrating light is passed throught the polychromator where it is split by the optical filters. The polychromator electronics produce fast and slow measurement of the light detected by each APD, the calibrating light is measured from the slow output and turned into electric signal. The spectral intensity is measured. In the fig.3.7, measured spectral transmission of polychromator filters is shown.

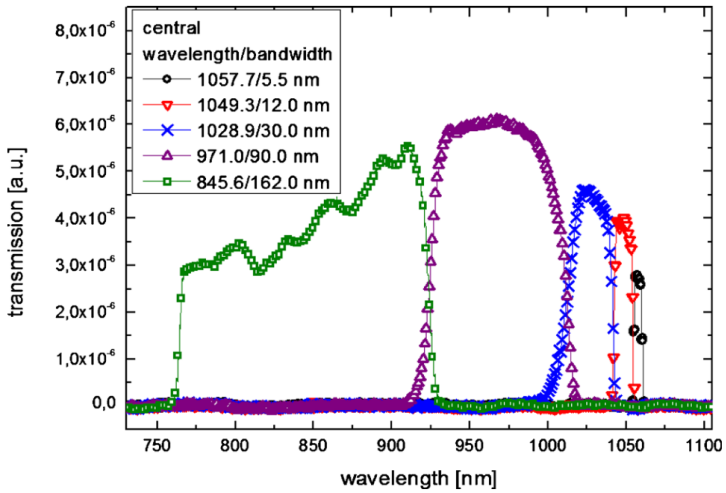

Figure 3.7: Transmission functions of the 5 spectral channels [17].

An iterative procedure has to be done in order to determine the electron temperature from the measurement. A convolution of the measured transmission functions with numerically simulated spectrum for a range of temperatures (fig.2.2) gives expected spectral channel ratio for each temperature (fig.3.7). The ratio is then iteratively compared with the actual ratio measured for each spatial point of TS diagnostics.

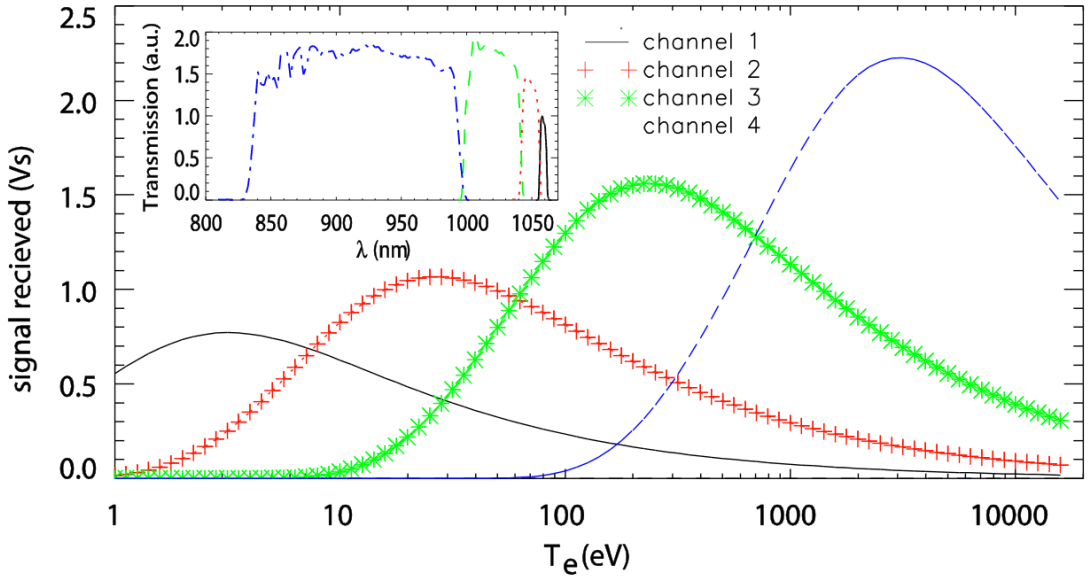

Figure 3.8: Ratio of the spectral channels as a function of electron temperature [courtesy Milan Aftanas].

Absolute density calibration

Detailed information regarding absolute calibration of TS systems can be found in [18]. Rayleigh or Raman scattering can be used for this purpose. On the COMPASS tokamak, Raman scattering is used, which has an advantage that the scattering radiation is at a different wavelength than the incident radiation. This feature allows the usage of the same arrangement as for TS measurements (Rayleigh scattering as calibration technique may need additional filters to deal with stray light radiation and Reyleigh scattering radiation). On the other hand Raman scattering needs precisely measured spectral calibration and the polychromator filters has to be designed with Raman calibration in mind. Nitrogen, oxygen, hydrogen or deuterium can be in principle used as a scattering gas. The nitrogen is used on the COMPASS tokamak.

The intensity of the scattered light is proportional to electron density through unknown system constants (local laser intensity, decay of the signal at the current set up of the optical system, etc.). By iterating the nitrogen pressure and measuring the scattered signal, the system constants required for calibration can be determined. Fig.3.9 shows normalized spectral transfer function of two spectral filters of polychromator together with expected anti-Stokes lines and laser line. Typical number of scattered photons integrated over the measured spectrum (only anti-Stockes lines are detected) are in range of thousands and tens of thousands for each spatial point/scattering volume for p=10 mbar.

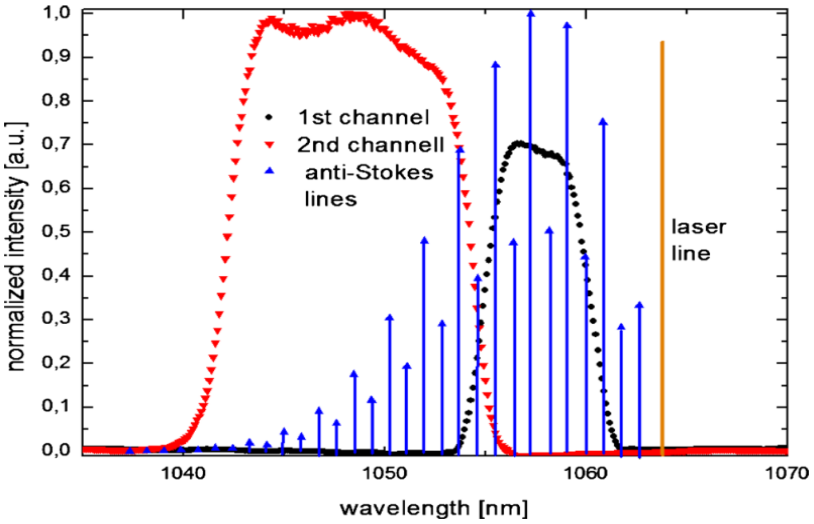

Figure 3.9: Expected Raman anti-Stokes lines from nitrogen for a vessel of 300 K temperature and normalized spectral transfer functions measured by polychromator [17].

4. Results

4.1 The edge pedestal

4.1.1 Motivation

F

One of the most important and challenging goals of fusion research is to understand the processes taking place in the plasma edge region. As it was mentioned in the theoretical part, during the high-confinement mode a region with a steep gradient of the plasma pressure occurs. It is a consequence of temporal suppression of the turbulent transport towards the walls in this area. A so-called edge transport barrier is formed, often referred to as the pedestal, as the core plasma parameters are raised up by the pedestal values. The formation of edge transport barrier on the profile of electron pressure is shown in Fig.4.1. The profile was reconstructed from the profiles of T_e and n_e from a selected plasma discharge. The black profile corresponds to L-mode and the blue profile was formed approximately 30 ms after it, when the plasma transited into H-mode. The top of the "pedestal" is at the $\psi_n = 0.9$. Some of the most important parameters of the corresponding discharge (plasma current, plasma density, D_α radiation and visible radiation) are shown in the fig.4.2 below. The plasma shot duration was 336.3 ms with the flat-top plasma current of 243.3 kA. The transition to H-mode was achieved by neutral beam injection with the output power of 256 kW, and it can be recognized on the sudden decrease of D_α signal at 1070 ms. H-mode period is ELM-free, lasts approximately 60 ms and then is terminated by H-L transition caused by impurity accumulation.

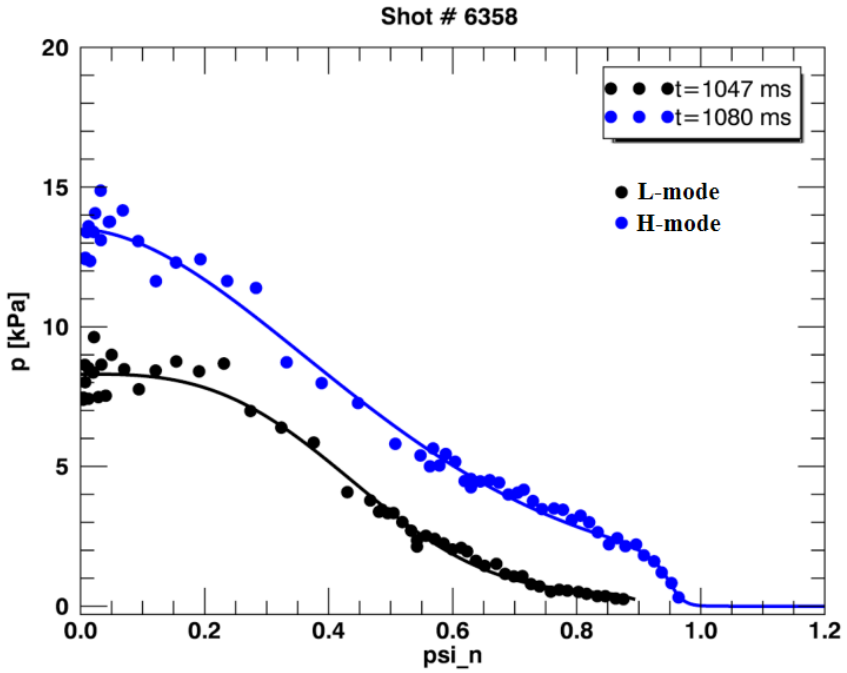

Figure 4.1: The formation of transport barrier on electron pressure (blue profile) during plasma discharge on the COMPASS tokamak.

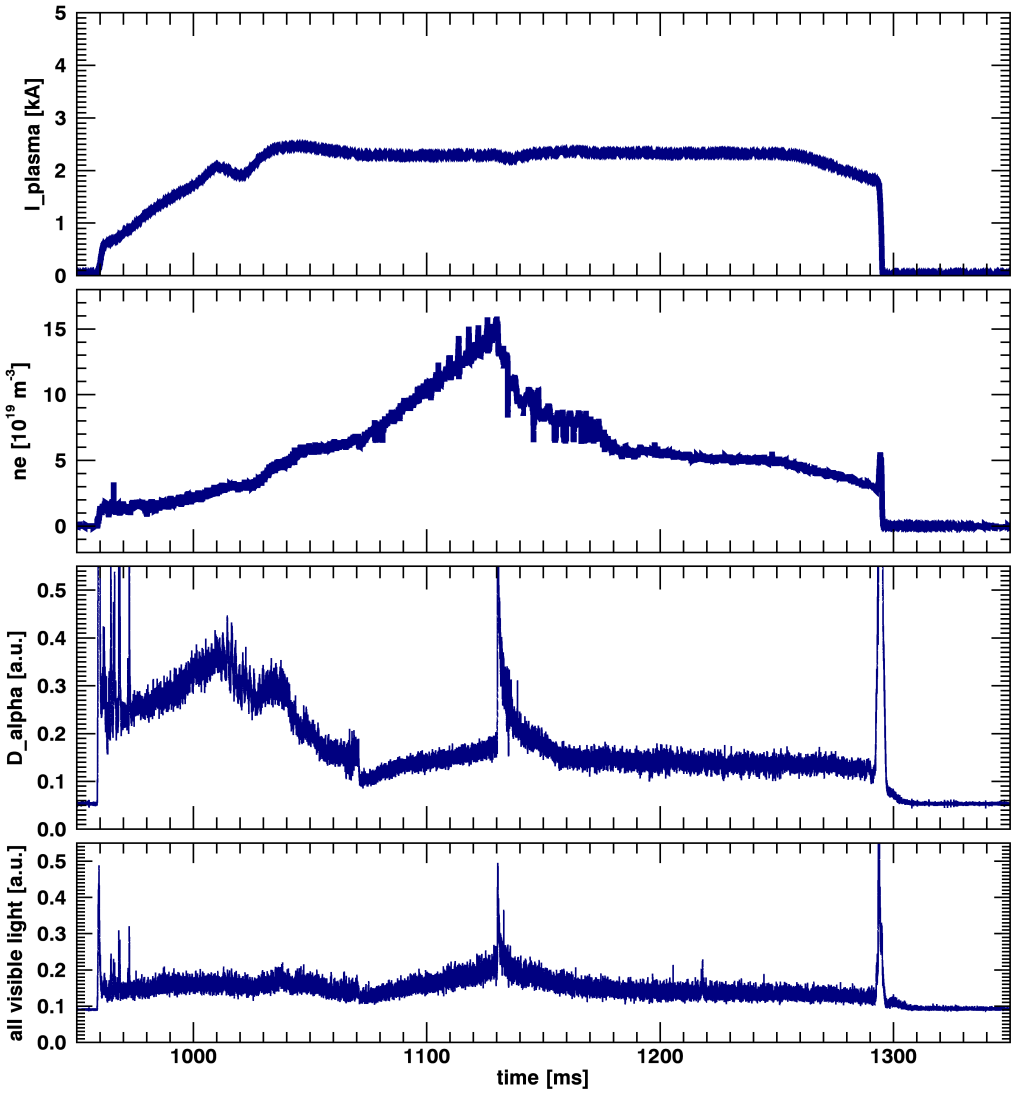

Figure 4.2: Evolution of the discharge #6358. From top to bottom: plasma current, plasma density, D_α radiation and visible radiation over the whole spectral range.

During H-mode, the global energy confinement time increases, as well as the energy stored in the plasma. In currently tested scenarios, it would be impossible to reach required efficiency for plasma confinement without transition to H-mode, and tokamaks would be no longer interesting as a future power plant solution. H-mode mode regime is therefore crucial, but unfortunately unstable.

If the gradient of pressure increases beyond a critical value, an instability occurs. There are various edge plasma instabilities affecting plasma confinement. One of the most dangerous type are the edge localised modes (ELMs), an MHD phenomena accompanying high performance tokamak regimes, as they cause a periodic collapse of the transport barrier leading to a rapid loss of energetic particles from the plasma. The changes induced by these instabilities happen on fast time scale ($\sim$ 1ms), therefore high precision spatial and temporal measurement is necessary. In case of bigger fusion devices like ITER, the ELMs (mainly type I ELMs) cause a significant power loads (current estimation of power re-

leased during one ELM is of the order 50 MW/m^2) towards the plasma-facing components that would lead to their immediate damage. A series of techniques (resonant magnetic perturbations, vertical kicks, etc.) are being investigated in order to find a way how to mitigate or suppress the ELMs, so they would cause less damage and the plasma confinement would be stabilised.

The complete theory of pedestal behavior in the H-mode and of the ELMs phenomena is still missing; it is not possible to credibly predict the pedestal characteristics for ITER. Therefore it is necessary to study the processes during formation of the edge transport barrier to which the instabilities are related. Furthermore, the pedestal width and stored energy are input to transport studies and scaling laws, so the edge density gradient is essential for understanding many edge dominated phenomena. The key plasma parameters, electron temperature and electron density, describing the transport barrier region, are measured by high-resolution Thomson scattering diagnostics at the COMPASS tokamak.

4.1.2 Measured profiles of electron temperature, density and pressure with pedestal

The typical profiles of electron temperature T_e and density n_e in ψ_n measured by TS diagnostics during an H-mode shot #6962 are in Fig.4.3. The profile of electron pressure p was reconstructed from the profiles of T_e and n_e. The parameters of the discharge are shown in the fig.4.4: there was a long H-mode during this discharge ($\sim$ 100 ms) varying between ELMy phase and ELM-free phase; the flat top plasma current reached 306.91 kA.

The central electron temperature typically reaches 0.7 - 1.5 keV, the central electron density usually varies between (1 - 2)$\times 10^{20} m^{-3}$ and is noticeably more flat than the temperature. The profile of electron pressure often looks very similar to the temperature profile. The typical pedestal height is 150 - 200 eV for electron temperature, (0.5 - 1)$\times 10^{20} m^{-3}$ for electron density and 1 - 3 kPa for electron pressure.

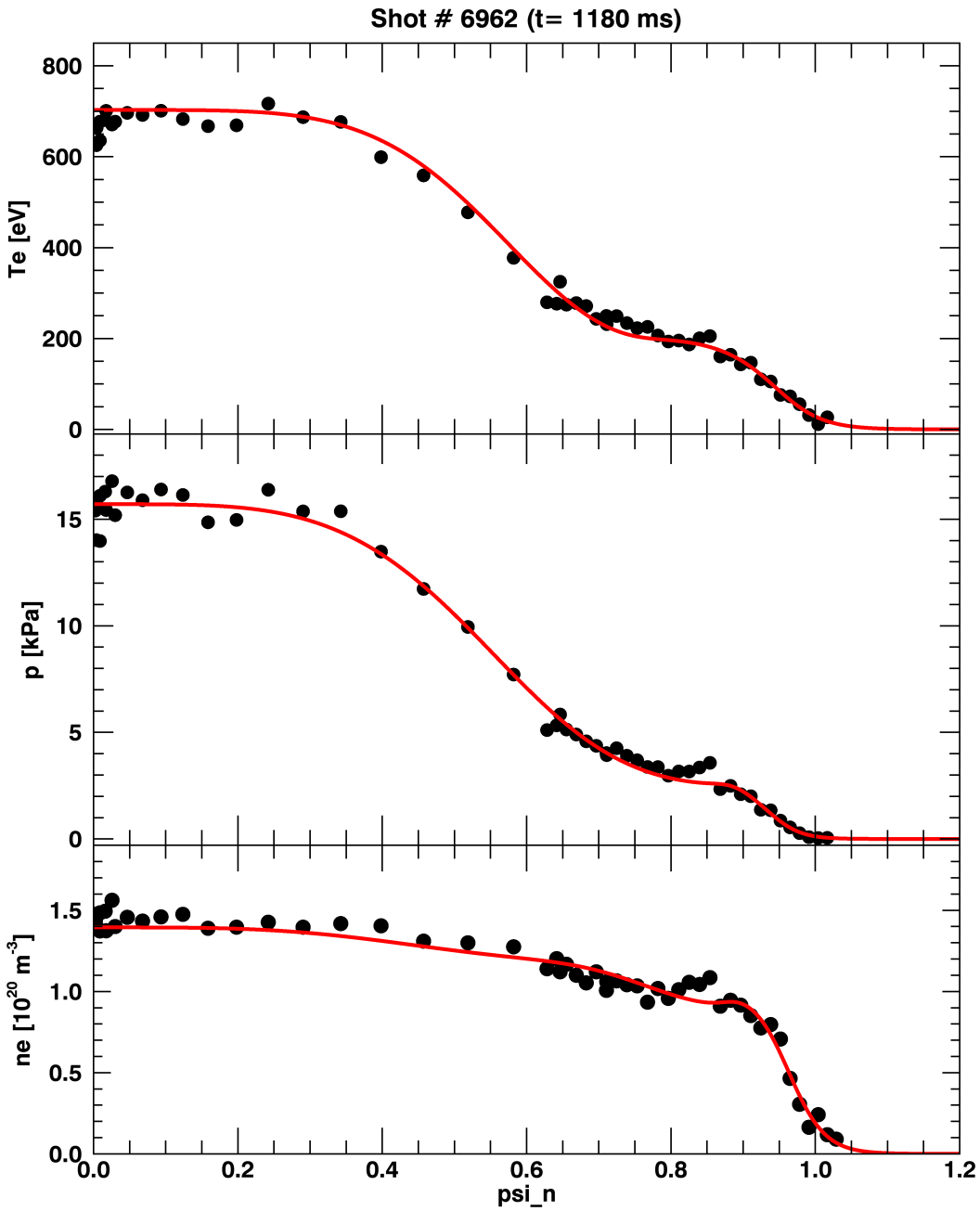

Figure 4.3: Full radial profiles of electron temperature, pressure and density in ψ_n for one laser shot during the plasma discharge #6962 measured by high resolution Thomson scattering on the COMPASS tokamak.

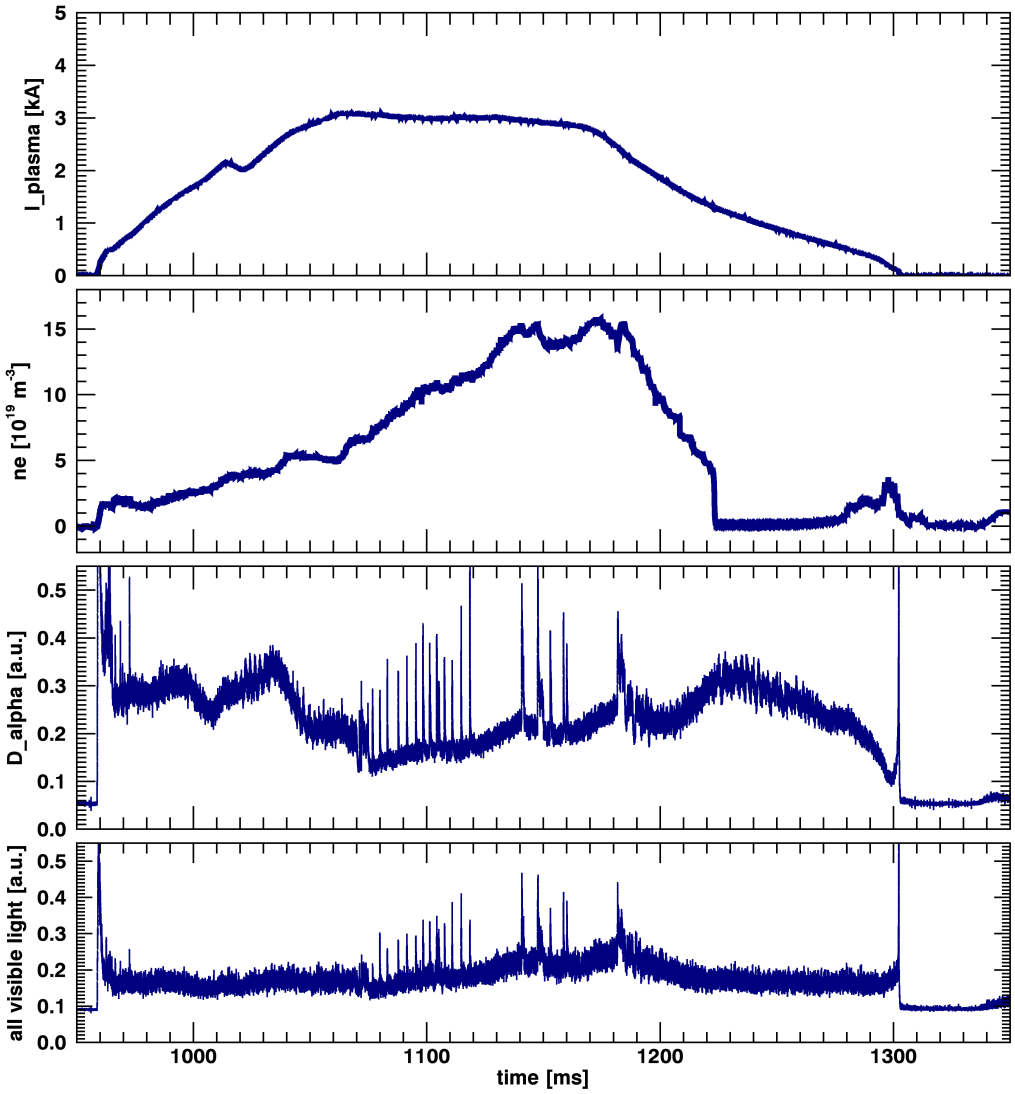

Figure 4.4: Evolution of the discharge #6962. From top to bottom: plasma current, plasma density, D_α radiation and visible radiation over the whole spectral range.

4.1.3 Edge pedestal fitting

It is generally accepted [12] that both the T_e and n_e pedestals are described by a modified hyperbolic tangent function (mtanh), a five parameter model described in [19]. The profiles of electron pressure can be fitted with mtanh as well, as they are obtained as a product of electron temperature and density. The mtanh function is a modification of tanh function, which is a natural shape of the edge density profile resulting from a simplification of the particle transport model. In [20] it is shown, that the n_e pedestal is described by the mtanh function, the profiles of T_e have been observed empirically to have this form. By fitting the transport barrier with mtanh function, important parameters such as the pedestal height b_{height} and width b_{width} can be determined. The other three parameters are the core slope b_{slope}, position of the pedestal b_{pos} and offset in the SOL b_{SOL}. The meaning of all the parameters and the shape of the mtanh function is illustrated

in the fig.4.5.

The equation that describes the shape of the edge transport barrier, obtained from [12], is:

$$F_{ped}(r;b) = \frac{b_{height} - b_{SOL}}{2}\left[\text{mtanh}\left(\frac{b_{pos} - r}{2b_{width}}, b_{slope}\right) + 1\right] + b_{SOL} \tag{4.1}$$

where the mtanh function is given by:

$$mtanh(x; b_{slope}) = \frac{(1 + b_{slope}x)e^{x} - e^{-x}}{e^{x} + e^{-x}} \tag{4.2}$$

This thesis follows the convention in the literature, where the pedestal width is considered as four times the fitted parameter b_{width}. The T_e and n_e pedestal widths then represent 76% of the pedestal to SOL fall-off [12].

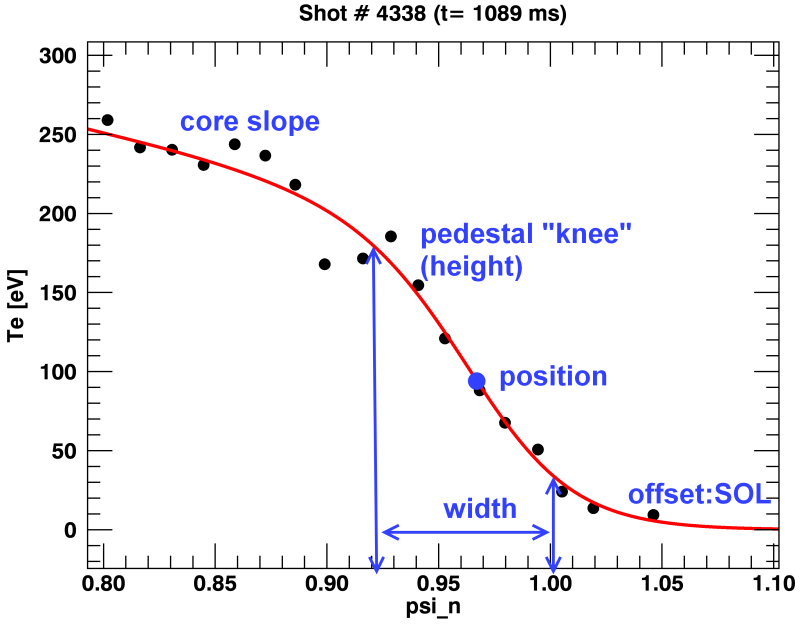

Figure 4.5: The mtanh function illustrated on the electron temperature profile from the shot #4338 with the parameters described in the picture.

4.1.4 Description of the fitting routine for the pedestal

The routine that is used for fitting of the edge pedestal profiles of T_e, n_e and p was written in IDL (Interactive Data Language) by the author of this thesis. The experimental data were read from the COMPASS Database (CDB), a virtual database created by J.Urban and J.Pipek. The fitting program also uses values of experimental data remapped from the vertical coordinate z to normalized psi ψ_n according to the assumption that the plasma parameters along magnetic surfaces are constant. This remapping is a part of the program EFIT 2D mapping written by V.Weinzettl.

The experimental profiles in ψ_n were taken as an input. In order to fit the pedestal parts of the profiles, IDL built-in function CURVEFIT was used. One of its arguments was a user-defined function "edge profile function", for which the equation (4.1) was taken. CURVEFIT uses a gradient-expansion algorithm to compute a non-linear least squares fit [21]. Iterations are limited either by reaching their maximal count (maximum number was set to 100), or by reaching χ^2 low enough.

The area of fitting and initial guess of four pedestal parameters have to be provided to the function. One of the parameters is fixed (usually the offset in SOL). The example of pedestal fitting of the experimental profile of electron temeperature is in the fig.4.6. The red line depicts the initial estimation of parameters, the green line is the resulting fit. The experimental values that are taken into account within the fitting area are depicted with black circles. When there is at least one experimental value at the pedestal fall-off, the resulting fit is stable even when the initial guess is relatively distant from the experimental values.

The core slope parameter varies with the chosen area of fitting because the dependence in the experimental profile is not linear; the angle of the resulting slope is therefore strongly dependent on it. The rest of parameters do not change.

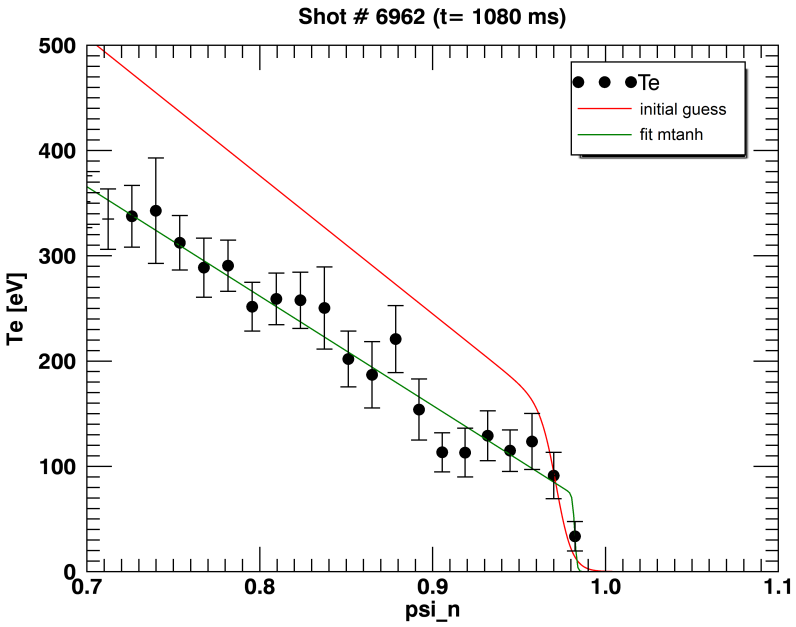

Figure 4.6: Example of electron temperature pedestal fitting of the profile from shot #6962. The red line represents initial guess of parameters of the mtanh function. The green line is the resulting fit.

4.2 Fitting of the full H-mode profiles of T_e, n_e and p

When fitting a full radial profiles of T_e, n_e and p, two methods were tested. Firstly, the core and the edge part of the profiles were fitted independently and

then averaged in the central region for smooth connection. The second method is fitting the profiles by a new single analytical function that was designed to fit in the COMPASS tokamak data. Both methods are described and compared in the following subsections. All fitting routines were written and tested by the author of this thesis.

4.2.1 Averaging of two independent fits

In this method, F_{ped} function was used for the edge part of the profile. The core region was fitted by a function:

$$F_{core}(r;a) = a_{ped} + [a_{height} - a_{ped}].\exp\left[-\left(\frac{r}{a_{width}}\right)\right]^{a_{exp}}, \tag{4.3}$$

where the exponential term was named a **"modified gauss function" (mgauss)**, as it is similiar to gauss function, but with a general power instead of square. The parameter a_{height} is illustrated in the fig.4.11 on the profile of electron temperature; the parameter a_{ped} means the pedestal height. The parameters a_{width} and a_{exp} change the width and the "flatness" of the mgauss function, respectively. The averiging function is of a weighted average shape:

$$F_{weight} = \alpha.F_{ped} + (1-\alpha).F_{core}, \tag{4.4}$$

where the α function is a smooth transition from 0 to 1 inspired by the Fermi-Dirac distribution. What is important to note, the described method works only for fitting of the profiles of electron temperature and electron pressure. For electron density a slight modification is used, where the the edge pedestal is fitted as described above, but the core region fit is a result of quotient of the core fits of T_e and p profiles. When these two fits are good, it usually also describes well the core part of the n_e profile.

The gaussian shape was chosen because the experimental profiles seemed to have this shape by sight; the second reason is that it also seemed convenient for the connection with the mtanh function. In the fig.4.7 the separate fits of core and edge region are depicted without any averaging. It is obvious, that these fits connect very well to each other and that the averaging does not change much their shape. The disadvantage of this method is that it is strongly dependent on the area of averaging.

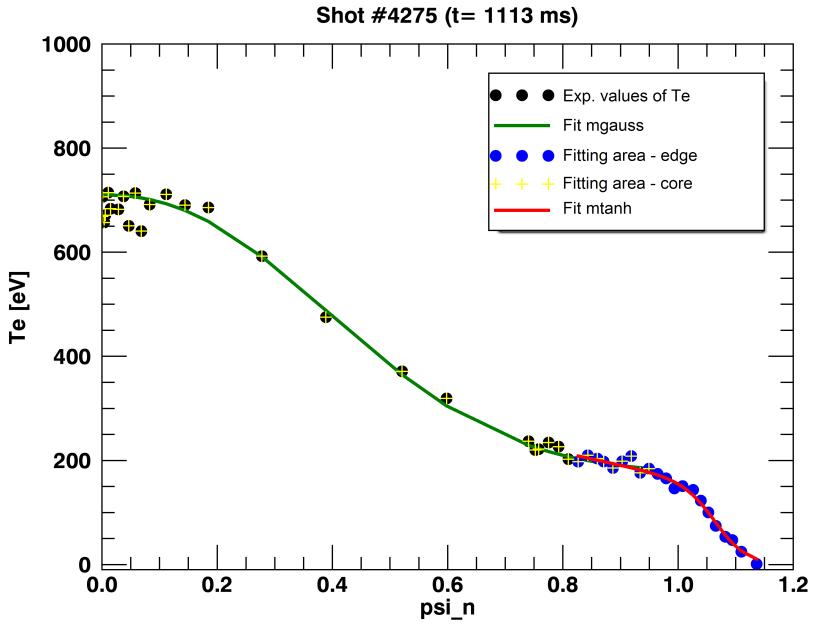

Figure 4.7: Example of fitting of the full profile from the discharge #4275 - separate fit of core region and pedestal. The fits are not connected. The area of fitting for both regions is distinguished by different colors.

In the figures 4.8, 4.9 and 4.10, the resulting fits of T_e, p and n_e with weighted average in the central region of the profile are shown.

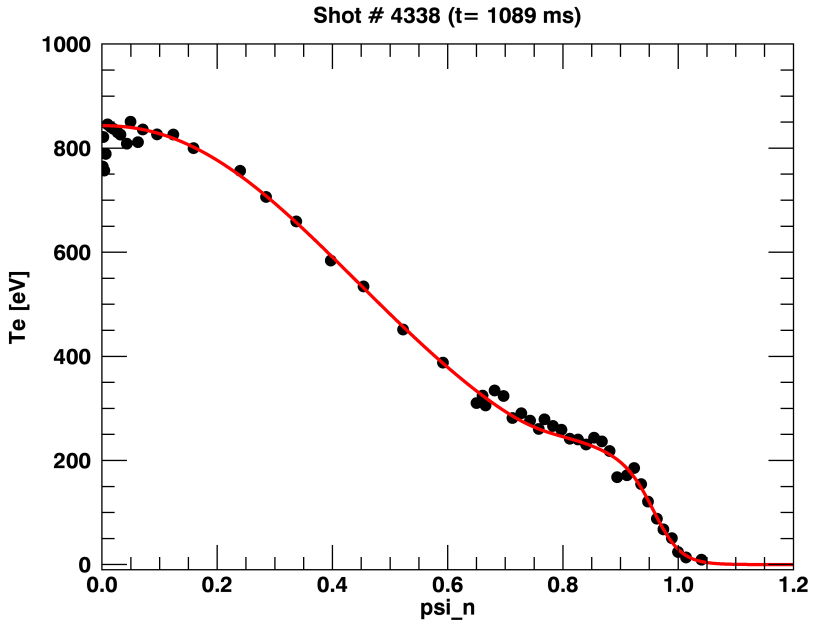

Figure 4.8: Example of fitting of the full profile of electron temperature from the discharge #4338 - weighted average in the central region.

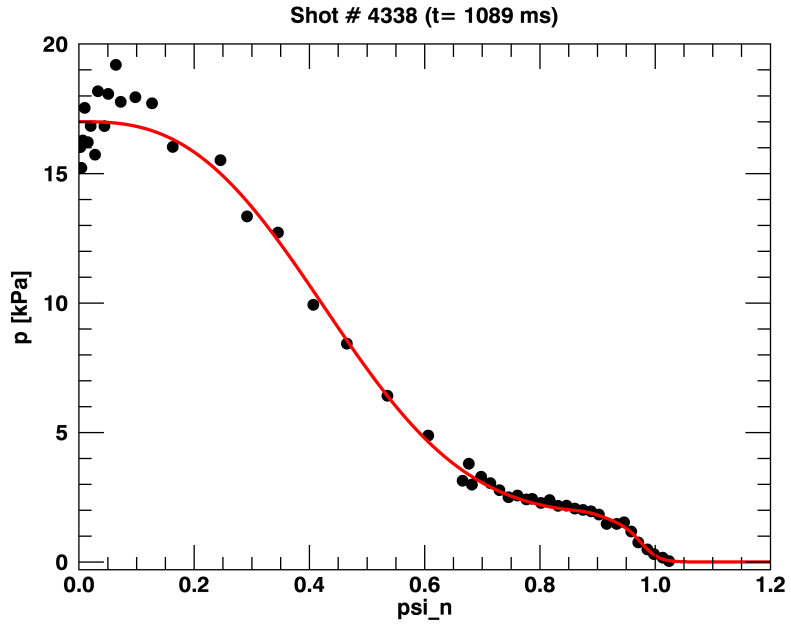

Figure 4.9: Example of fitting of the full profile of electron pressure from the discharge #4338 - weighted average in the central region.

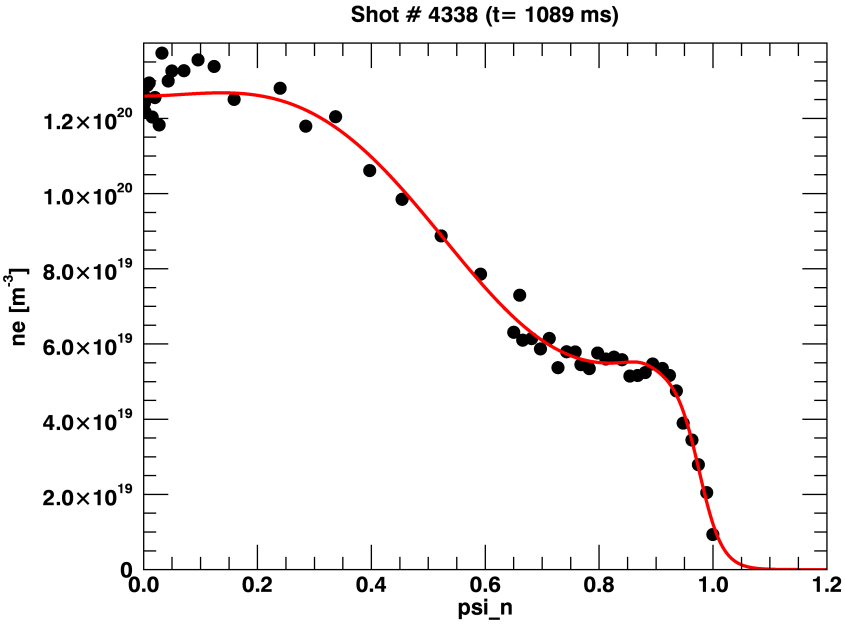

Figure 4.10: Example of fitting of the full profile of electron density from the discharge #4338 - weighted average in the central region.

4.2.2 Single analytical fit method

The function for fitting of the full profiles of electron temperature, density and pressure measured by TS diagnostics was developed to fit the COMPASS tokamak

data and was presented for the first time at the SPPT conference in Prague, June 2014 [22]. Profiles of T_e, n_e and p in ψ_n are well fitted by a single empirical function:

$$F_{analytical}(r; a, b) = F_{ped}(r; b) + [a_{height} - F_{ped}(r; b)].\exp\left[-\left(\frac{r}{a_{width}}\right)\right]^{a_{exp}}, \quad (4.5)$$

where F_{ped} is the edge profile function (4.1) based on mtanh, the exponential term is mgauss function explained in the previous subsection, the parameter a_{height} has the same meaning as in the eq.(4.3) and is illustrated in the fig.4.11 on the profile of electron temperature.

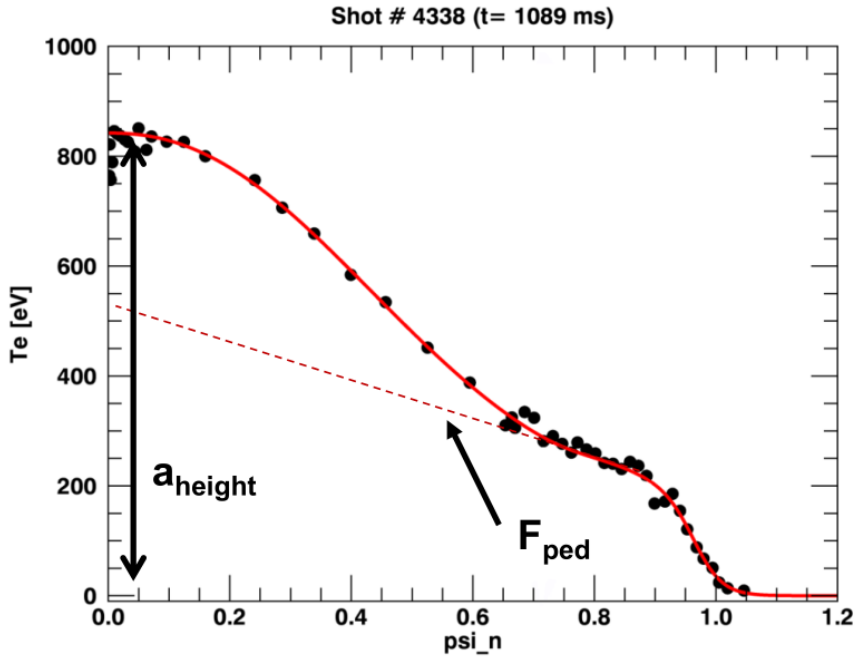

Figure 4.11: Profile of electron temperature fitted with analytical function with explanation of terms in eq.().

The function $F_{analytical}$ has 10 parameters in total - 5 for the mgauss and 5 pedestal parameters, but uses only 7 as some of them are variable in practice, the rest is set as constant. The position of the maximum is fixed to zero, the parameter a_{ped} is also fixed within the core parameters, the SOL height is fixed to zero as well. First, the edge pedestal is fitted from all the experimental data. Then these pedestal parameters together with initial estimation of the core parameters are taken as a input to $F_{analytical}$. This function is then fitted several times, each time releasing some of the parameters, and improving the resulting fit. At the end, all the parameters are released, including the parameter b_{slope} (one of the pedestal parameters called the core slope), which influences the connection with the core gauss function. The program enables to decide whether to release this last parameter or not, sometimes the resulting fit is better without it. The great advantage of this method apart from the fact that it is a single analytical function is that it does not matter on the chosen area of fitting anymore, and therefore the fit is very stable. The previous method was very much dependent on the quality

of the fits of electron temperature and pressure; when the fits were not good, the resulting fit of the electron density was often wavy (as seen in the fig.4.15 in the subsection comparing the two fitting methods). This analytical method gives good results and describes well even the very flat profiles of electron density.

What is also important to note, the single analytical fit is advantageous for further data processing. It can be easily analytically differentiated, what is used for example as an input to numerical codes that calculate the tokamak stability diagram.

The usage of this new fitting function on the experimental profiles of electron temperature, pressure and density is demonstrated in the fig.4.12. In the following fig.4.13 the same profiles are shown with zoom to the pedestal region.

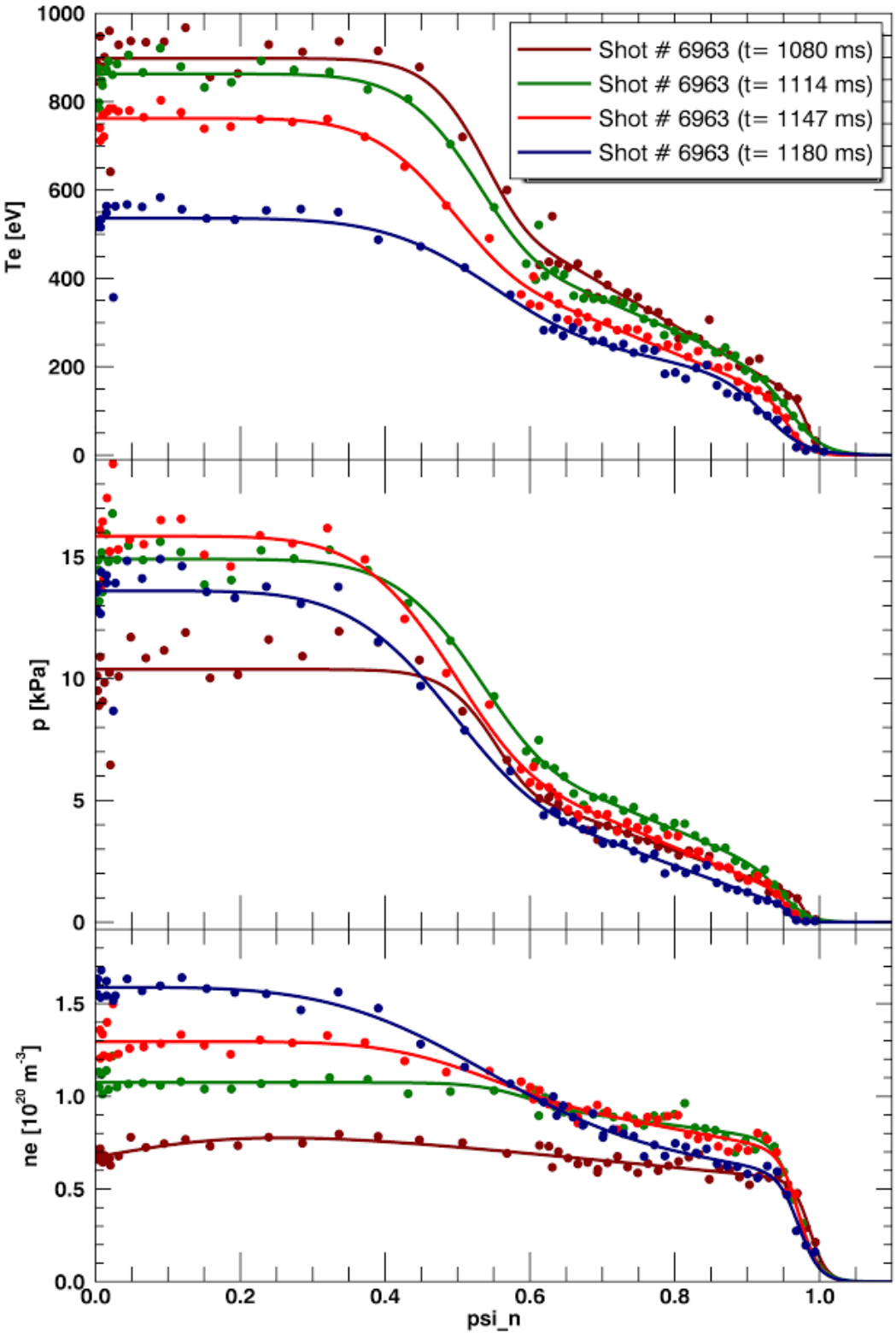

Figure 4.12: Full radial profiles of electron temperature, pressure and density in ψ_n for several laser shots during the plasma discharge #6963 measured by high resolution Thomson scattering on the COMPASS tokamak and fitted by single empirical function.

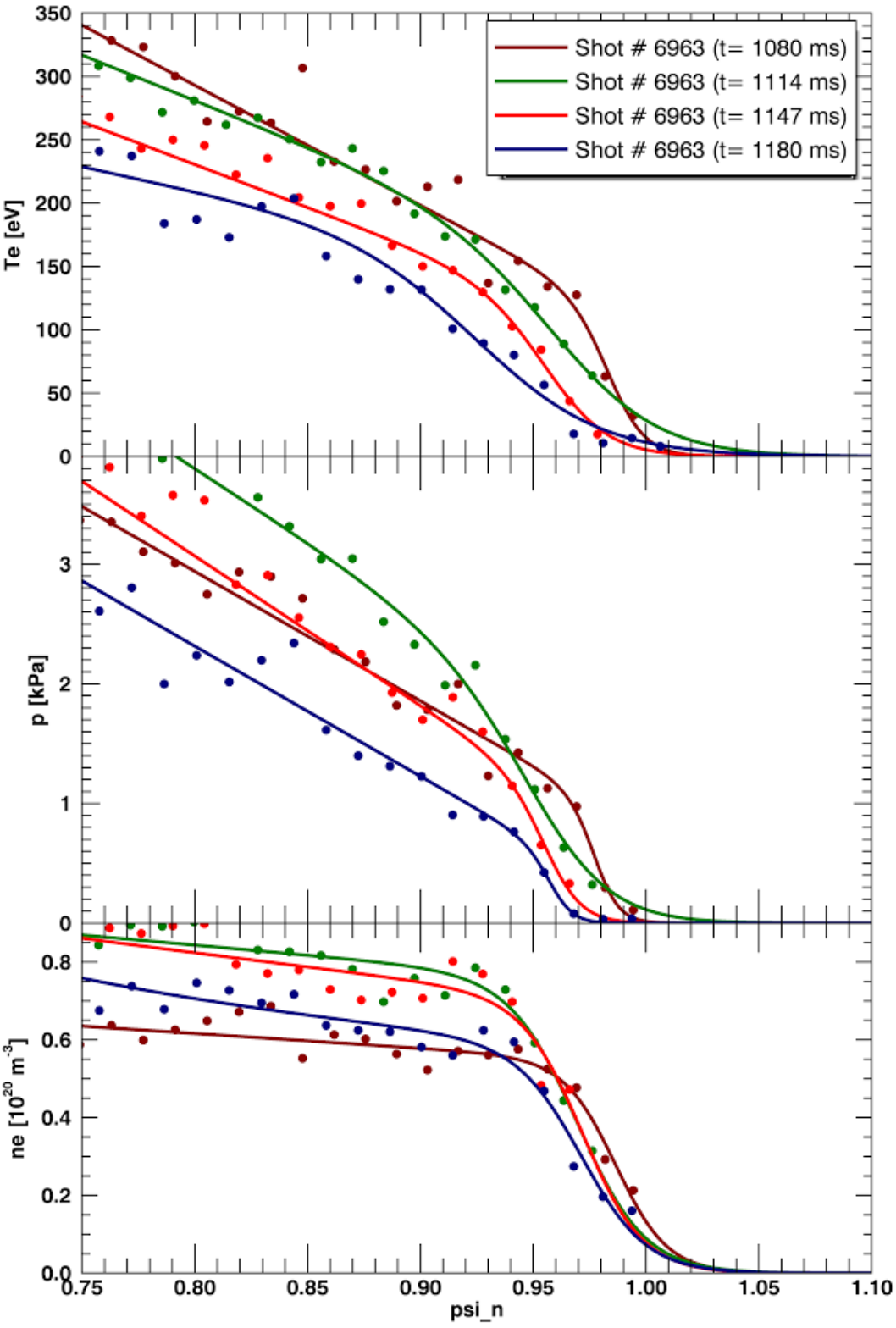

Figure 4.13: Zoom on pedestal profiles of electron temperature, pressure and density from the previous fig.4.12.

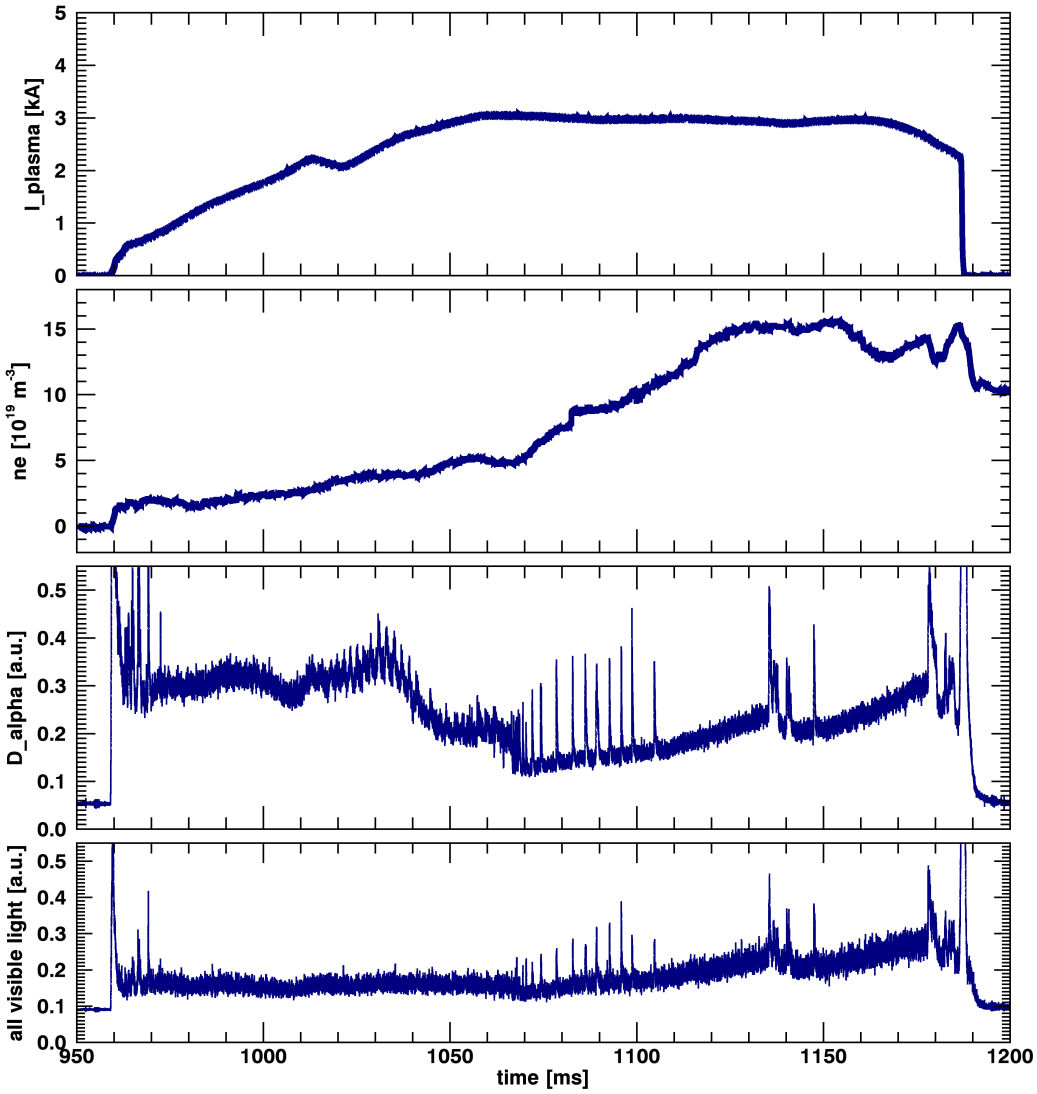

Figure 4.14: Evolution of the discharge #6963. From top to bottom: plasma current, plasma density, D_α signal and visible radiation over the whole spectral range.

The parameters of the corresponding discharge are shown in the fig.4.14. There was a long H-mode that started with big ELMs followed by an ELM-free period, which was interrupted by several ELMs and then again continued as ELM-free. The flat top plasma current reached 305.93 kA.

4.2.3 Comparison of the two methods for full profile fitting

In the following figures 4.15 and 4.16, the two methods for full profile fitting are compared by fitting the same experimental data from the shot #6962. Both methods visually follow the data well. The most significant difference is in the fit of electron density, where the analytical fit appears more suitable. The area for pedestal fitting was too small and does not follow the data well in the region of psi_n=(0.7,0.9) in the case of averaged fit. Another difference can be seen on the

profiles of electron temperature, where using the weighted averaging method the connection of the two fits is visibly worse due to the core slope parameter b_{slope}.

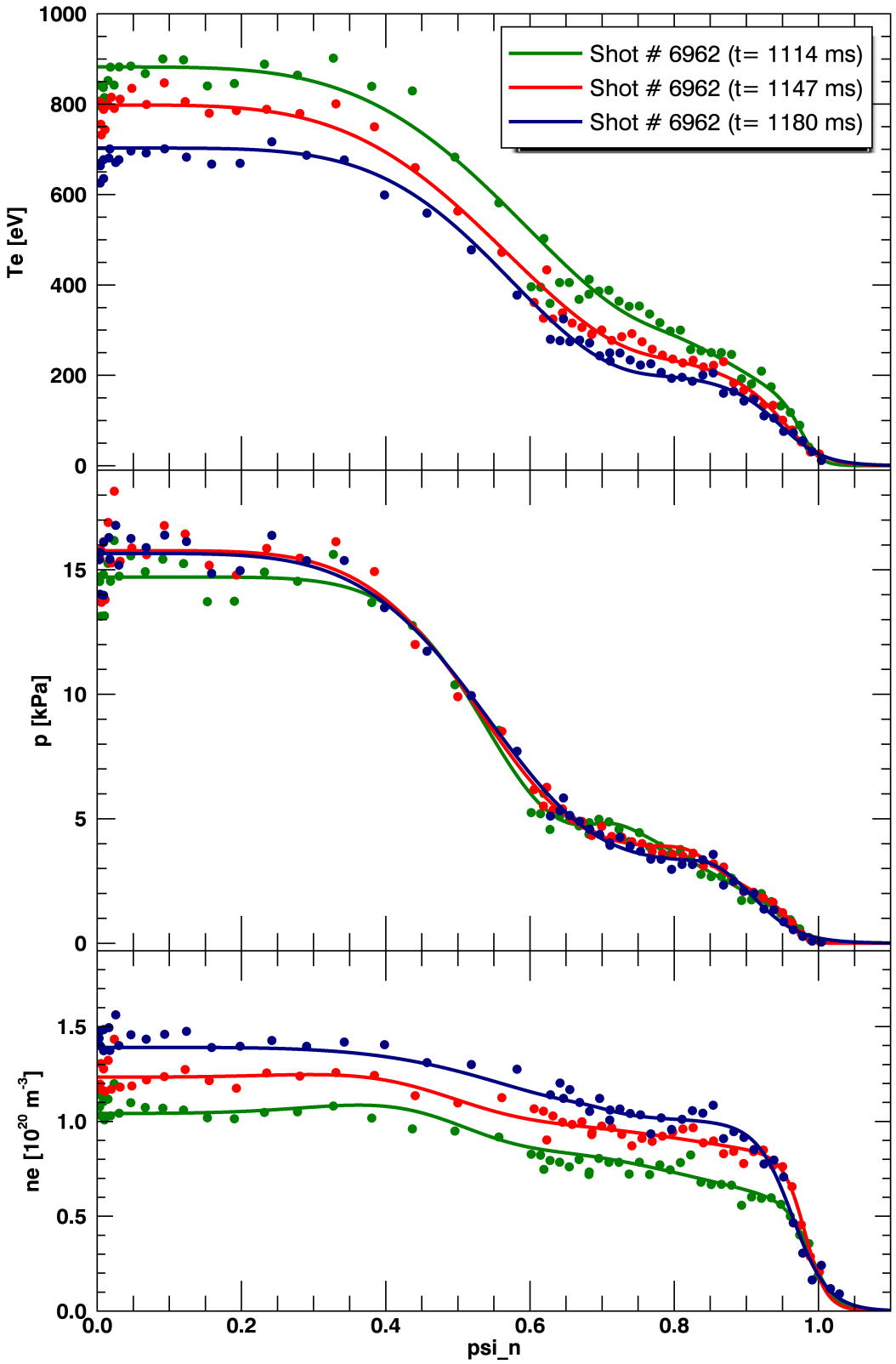

Figure 4.15: Experimental profiles of T_e, n_e and p from the discharge #6962 fitted by averaging of two independent fits.

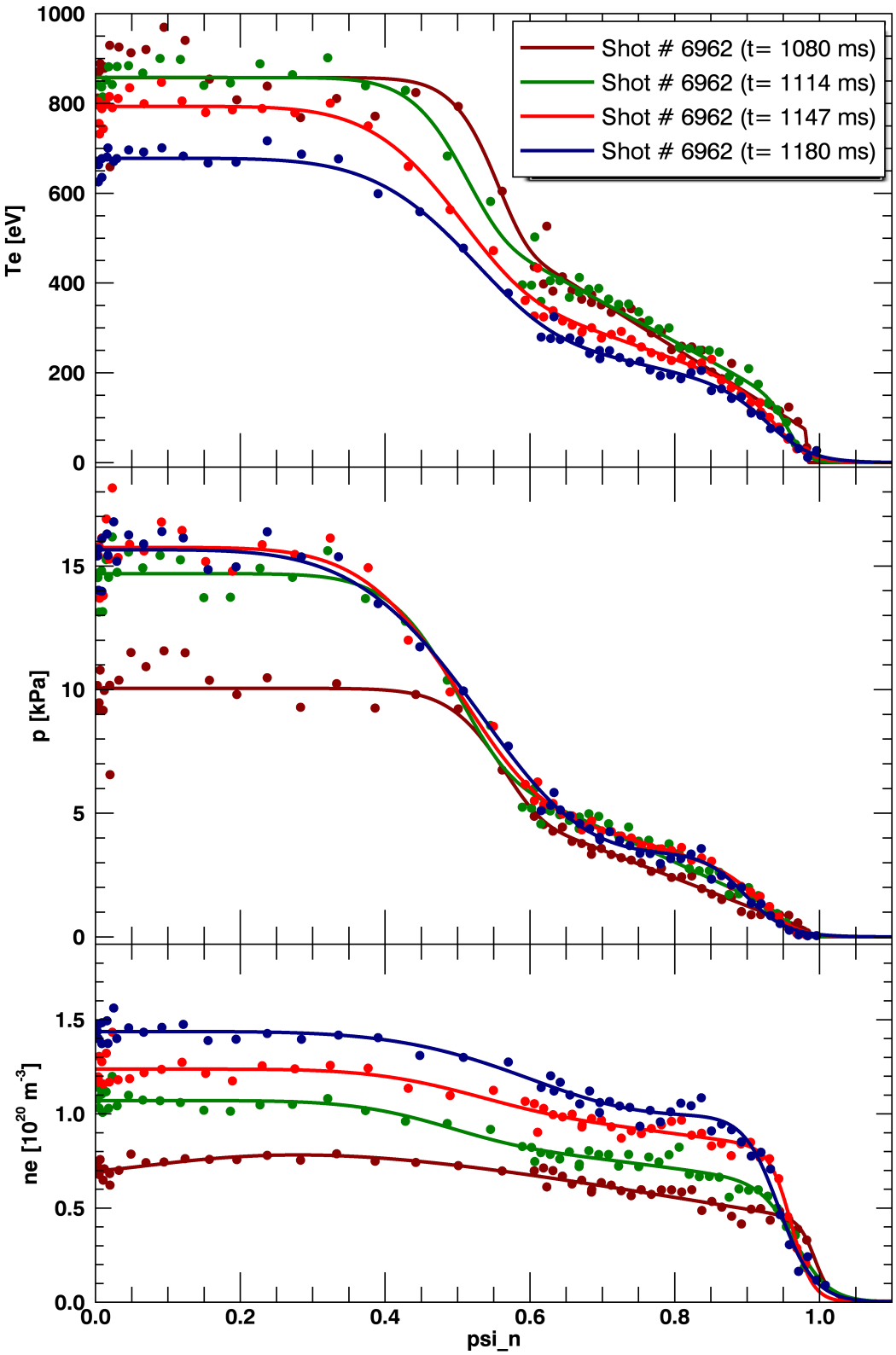

Figure 4.16: Experimental profiles of T_e, n_e and p from the discharge #6962 fitted by single analytical fit.

4.3 Searching for L-H threshold

In order to find a possible threshold of pressure for the transition between L-mode and H-mode (L-H transition), or different transitions for various types of H-modes, a set of COMPASS shots was statistically processed. Particularly, diagram of electron temperature versus electron density was studied, where fitted values of T_e and n_e on approximated value of top of the pedestal (ψ_n=0.9) were used according to analysis on MAST tokamak (fig.4.17, courtesy Rory Scannell).

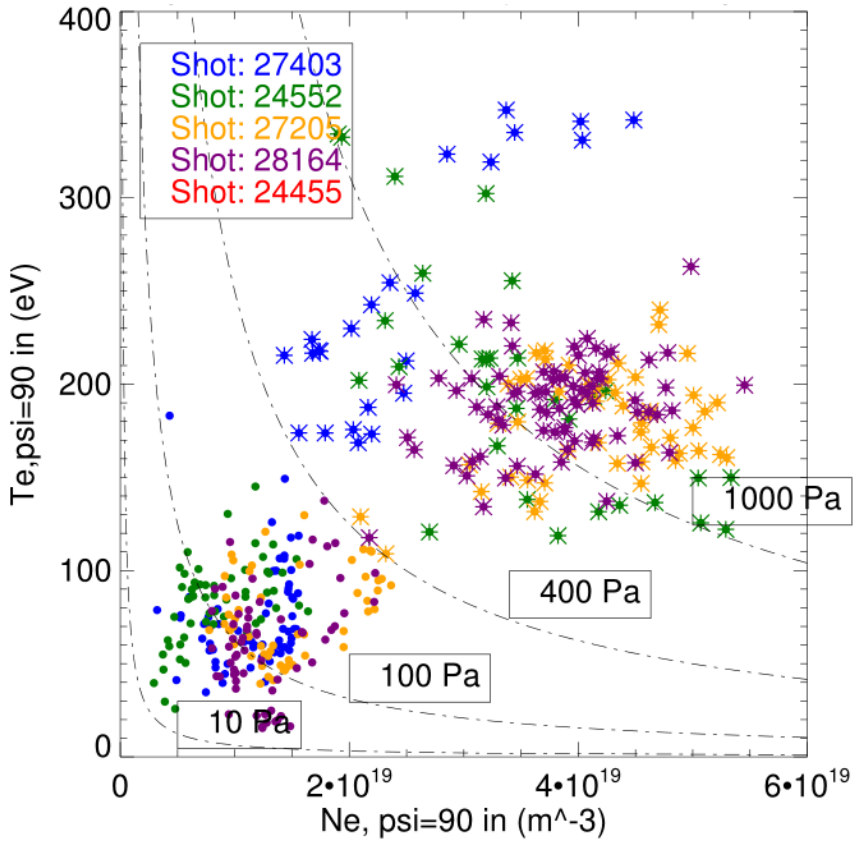

Figure 4.17: Electron temperature vs. density at $\psi_n = 0.9$. Data from MAST tokamak (courtesy Rory Scannell).

Resulting diagram for the COMPASS tokamak is in the fig.4.18. 37 COMPASS shots were processed with Ohmic, ELM-free, ELMy, NBI heated and RMP (resonant magnetic perturbations) H-mode regimes. The data was taken from the quasi-stationary state of the discharges. One point in the figure corresponds to one temporal record of the TS measurement during the selected discharge; each shot is depicted in different color and records in L-mode and H-mode are distinguished by circle and star symbols, respectively. The clear pressure threshold on the contrary to MAST data could not be recognized from the figure. Even though the borderline of p=1200 Pa separates the major part of L/H data, some H-mode records fall into region with lower pressure, but higher temperatures than L-mode records. However, in a closer look, **a borderline for temperature can be observed around 150 eV.**

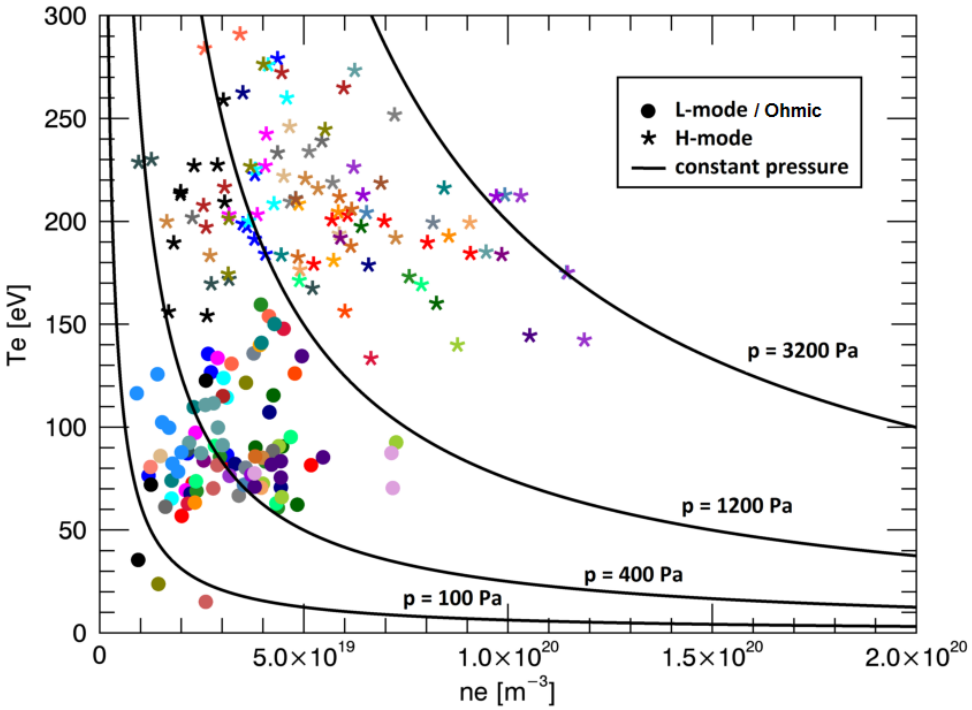

Figure 4.18: Electron temperature vs. density at $\psi_n = 0.9$ were statistically processed for 37 COMPASS tokamak shots.

Another analysis was made in order to find out, what could cause the "shift" of some of the H-mode data to lower pressures. The NBI heated H-modes were spread rather randomly in the diagram. The idea was to look at H-mode regime with ELMs, because as they cause a sudden collapse of transport barrier, this also means the drop in pressure (and density) until the barrier "recovers". In the fig.4.19 the same data was used, but depicted in different colors. Now all of the L-mode data are pink; the H-mode records that are ELM-free are dark dark blue, and the H-mode records with ELMs are green. The tendency to shift to lower densities with ELMs is obvious; however, some ELM-free records are still in the lowest density region.

It is also important to emphasise, that some discharges have a "mixed" H-mode regime, where the ELM-free period and ELMs alternate. This might also cause that records corresponding to "mixed" regime would take place in the lower density region of the diagram. It is due to the fact, that ELMs, depending on their strength, carry a certain amount of energy with them and the transport barrier does not recover quickly enough to its original form; and so this kind of the ELM-free period might be different from the "pure" ELM-free one. In the fig.4.20 this alternating type of H-mode was distinguished with light blue color; the rest (pink L-mode, dark blue color for ELM-free records only, and green color for H-mode with ELMs during the whole period) stays the same. The ELM types were not taken into account in this analysis. Recently, it has been proved that the COMPASS tokamak is able to achieve the type I ELMs, but further analysis is required.

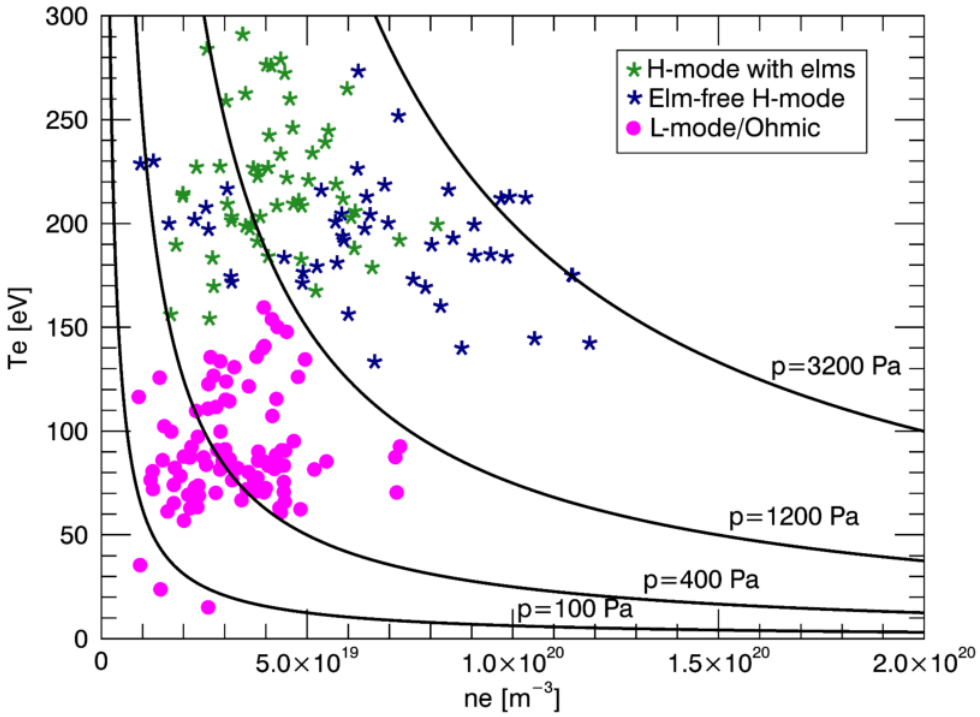

Figure 4.19: Electron temperature vs. density at $\psi_n = 0.9$ were statistically processed for 37 COMPASS tokamak shots. H-mode records with ELMs are distinguished by green symbols.

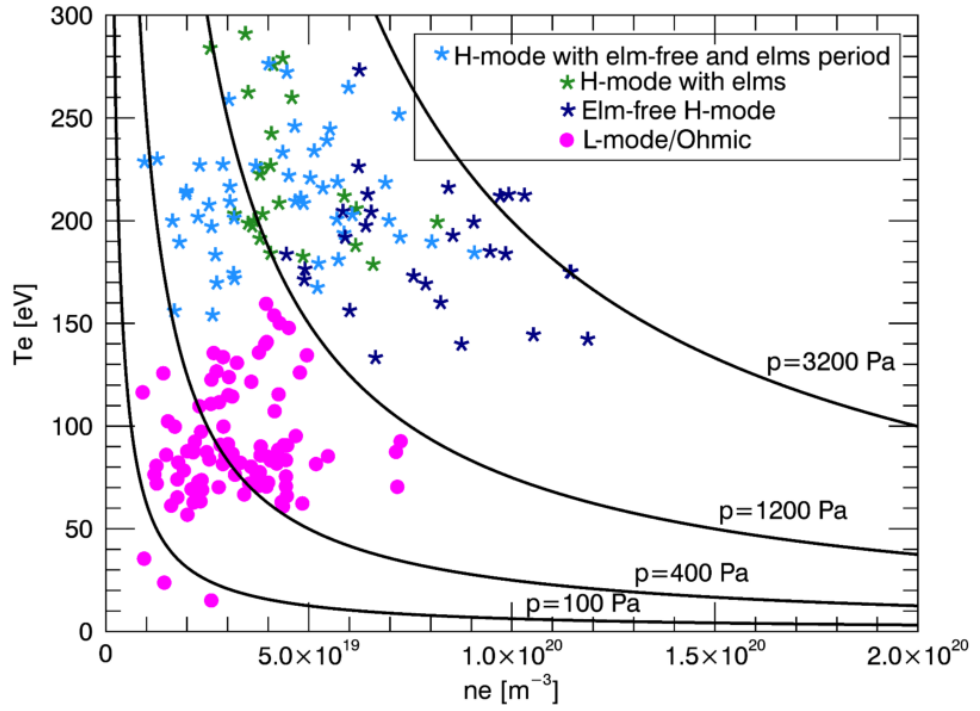

Figure 4.20: Electron temperature vs. density at $\psi_n = 0.9$ were statistically processed for 37 COMPASS tokamak shots. H-modes with alternating ELMs and ELM-free period are distinguished by light blue symbols.

4.4 Confinement time

The energy confinement time τ_E is one of the important plasma parameters. It is defined by the global energy confinement:

$$\frac{dW(t)}{dt} = P_{OH} - \frac{W(t)}{\tau_E}, \tag{4.6}$$

where P_{OH} is plasma heating power and $W(t)$ is total energy of the plasma of both the electron and ion compoment, given by kinetic energy of the particles:

$$W(t) = \int \frac{3}{2} k(n_e(t)T_e(t) + n_i(t)T_i(t))dV. \tag{4.7}$$

The electron temperature and density are measured by TS diagnostics. For ion component in purely ohmically heated plasma we can make an assumption, that due to higher mobility of electrons, it contributes to the total energy by $\frac{1}{3}$ of the electron energy [23]. The ohmic heating power P_{OH} is given by

$$P_{OH} = I_{plasma}.U_{res}, \tag{4.8}$$

where I_{plasma} is the plasma current and U_{res} is the resistive part of loop voltage on the plasma torus. Plasma current is measured by magnetic diagnostics. U_{res} is not measured directly, but it can be determined from relation

$$U_{res} = U_{loop} - L\frac{dI_{plasma}}{dt}, \tag{4.9}$$

where loop volage U_{loop} is measured by a flux loop surrounding the tokamak vessel, and the inductance L is approximately $1\mu H$. The time derivative of $W(t)$ is estimated from the comparison of two subsequent measurements. The evolution of τ_E for the discharge #6963 is shown in fig.4.21 In the quasi-stationary phase of the discharge it varies between 12 and 21 ms.

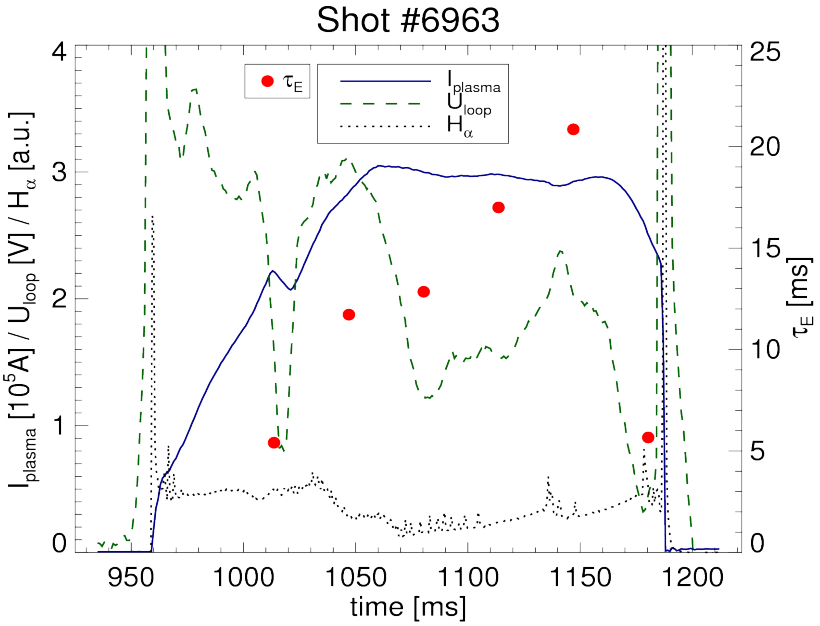

Figure 4.21: Evolution of τ_E values for the discharge #6963.

4.5 Estimation of effective charge number Z_{eff}

The effective charge number Z_{eff} can be estimated using profiles of electron temperature measured by high-resolution TS and plasma resistivity, as it depends upon temperature. The classical, or Spitzer, conductivity of plasma applies when the collisionality of plasma is high. The plasma resistivity is then equal to Spitzer resistivity and is given by [23]:

$$\eta_{Spitzer} = 2.8 * 10^{-8} Z_{eff} T_e^{3/2}, \tag{4.10}$$

where the electron temperature T_e is in keV. The neoclassical theory predicts [24] under certain conditions the existence of so-called banana particles which are trapped in the magnetic field. This effect is expressed in the neoclassical correction η_{neo} and applies for low collisionalities [24]. Neoclassical resistivity can be calculated as

$$\eta_{neo} = \frac{\eta_{spitzer}}{\left(1 - \sqrt{\frac{r}{R}}\right)^2}, \tag{4.11}$$

where r corresponds to vertical coordinate z and $R = 0.56$ m is tokamak major radius. In contrast to the Spitzer resistivity, the neoclassical resistivity has an aspect-ratio dependence. Z_{eff} can be estimated from comparison with equation for mean resistivity:

$$\eta = \frac{U_{loop} \pi a^2}{2\pi R I_{plasma}}, \tag{4.12}$$

where $a = 0.2$ m is tokamak minor radius. The estimated values of Z_{eff} using Spitzer resistivity for the discharge #6963 are in the fig.4.22

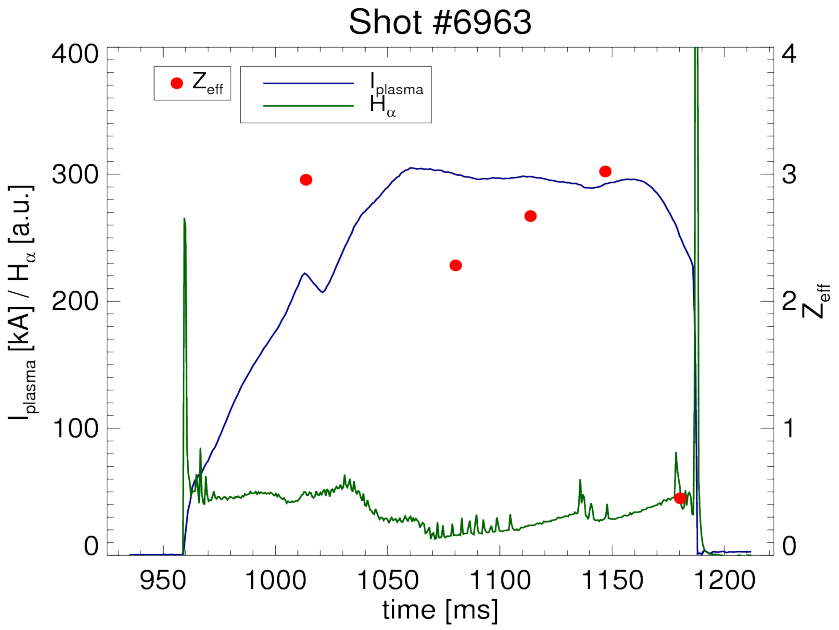

Figure 4.22: Evolution of the Z_{eff} values for the discharge #6963.

Conclusion

In this thesis, the analysis of experimental data measured by high-resolution Thomson scattering diagnostic system on the COMPASS tokamak was presented. The most interesting experimental results were obtained from the edge TS system. Its high spatial resolution and temporally localized measurements enables to study the edge transport barrier, an interesting phenomena that is formed in plasma during the tokamak operational regime with high-confinement. Understanding the physics behind the formation of the transport barrier and of instabilities that are closely bound to it is a key factor for operating next step fusion devices.

A convenient technique of pedestal fitting by mtanh was applied on the COMPASS tokamak H-mode edge profiles of electron temperature and density. A new technique of fitting of the full radial profiles of T_e, n_e and p was introduced either by fitting of the core and the edge profiles independently, or more elegantly by a single analytical function. Both approaches give good results, but in some cases (mostly for electron density) the analytical fit is more suitable as it is not depedent on the resulting fits of the electron temperature and pressure. What is more, it can be used in further data processing, e.g. calculating the tokamak stability diagram.

Using the fitting, the diagram of electron temperature versus electron density on ψ_n=0.9 for various types of COMPASS tokamak shots was studied. A clear threshold in pressure for the L-H transition could not be recogized, but a borderline in temperature around 150 eV was observed. The influence of ELMs on the position of data in the diagram was studied. It was obvious, that ELMs cause a shift to lower densities due to sudden collapse of the edge transport barrier. The alternating ELMy and ELM-free H-mode has this effect as well because the transport barrier does not recover quickly enough after ELM phase to not to influence the ELM-free phase of the H-mode.

In the last part of the results, the estimation of other important plasma parameters derived from TS data, the confinement time τ_E and effective charge number Z_{eff}, has been shown.

Bibliography

[1] "en.wikipedia.org/wiki/nuclear_fusion."

[2] "users.jet.efda.org."

[3] F. Wagner, G. Becker, K. Behringer, D. Campbell, A. Eberhagen, W. Engelhardt, G. Fussmann, O. Gehre, J. Gernhardt, G. v. Gierke, G. Haas, M. Huang, F. Karger, M. Keilhacker, O. Klüber, M. Kornherr, K. Lackner, G. Lisitano, G. G. Lister, H. M. Mayer, D. Meisel, E. R. Müller, H. Murmann, H. Niedermeyer, W. Poschenrieder, H. Rapp, H. Röhr, F. Schneider, G. Siller, E. Speth, A. Stäbler, K. H. Steuer, G. Venus, O. Vollmer, and Z. Yü, "Regime of improved confinement and high beta in neutral-beam-heated divertor discharges of the asdex tokamak," *Phys. Rev. Lett.*, vol. 49, pp. 1408–1412, Nov 1982.

[4] J. P. Freidberg, *Plasma Physics and Fusion Energy*. Cambridge University Press, 2007. Cambridge Books Online.

[5] J. Thomson, "Lxx. on the number of corpuscles in an atom," *Philosophical Magazine Series 6*, vol. 11, no. 66, pp. 769–781, 1906.

[6] A. J. H. Donné, C. J. Barth, and H. Weisen, "CHAPTER 4: LASER-AIDED PLASMA DIAGNOSTICS," *Fusion Sci. Technol.*, vol. 53, no. 2, pp. 397–430, 2008.

[7] G. Fiocco and E. Thompson, "Thomson scattering of optical radiation from an electron beam," *Phys. Rev. Lett.*, vol. 10, pp. 89–91, Feb 1963.

[8] E. Fuenfer, B. Kronast, and H.-J. Kunze, "Experimental results on light scattering by a /theta/-pinch plasma using a ruby laser," Jun 1963.

[9] N. Peacock, D. Robinson, M. Forrest, and P. Wilcock, "Measurement of the electron temperature by thomson scattering in tokamak t3," *Nature*, vol. 224, pp. 488–490, 1969.

[10] E. E. Salpeter, "Electron density fluctuations in a plasma," *Phys. Rev.*, vol. 120, pp. 1528–1535, Dec 1960.

[11] S. Prunty, "A primer on thomson scattering theory for high-temperature fusion plasmas." material for Hands on Thomson Scattering Workshop, 2013.

[12] R. Scannell, *Investigation of H-mode Edge Profile Behaviour on MAST Using Thomson Scattering*. NUI, 2007 at Department of Electrical and Electronic Engineering, UCC., 2007.

[13] A. Selden, *Simple Analytic Form of the Relativistic Thomson Scattering Spectrum, Jan. , 1982*. Report, AEA Technology, Atomic Energy Research Establishment, 1982.

[14] P. Böhm, *Časo-prostorový vývoj plazmatu v tokamaku COMPASS*. PhD thesis, České vysoké učení technické, Fakulta jaderná a fyzikálně inženýrská, 2011.

[15] P. Böhm, P. Bilkova, M. Aftanas, E. Štefániková, O. Mikulín, R. Melich, F. Janky, J. Havlíček, D. Šesták, V. Weinzettl, J. Stöckel, M. Hron, and R. Panek, "Edge thomson scattering diagnostic on compass tokamak - installation, calibration, operation, improvements," in *20th Topical Conference on High-Temperature Plasma Diagnostics*, June 2014.

[16] P. Bílková, M. Aftanas, P. Böhm, V. Weinzettl, D. Šesták, R. Melich, J. Stöckel, R. Scannell, and M. Walsh, "Design of new thomson scattering diagnostic system on {COMPASS} tokamak," *Nuclear Instruments and Methods in Physics Research Section A: Accelerators, Spectrometers, Detectors and Associated Equipment*, vol. 623, no. 2, pp. 656 – 659, 2010. 1rs International Conference on Frontiers in Diagnostics Technologies.

[17] P. Bilkova, R. Melich, M. Aftanas, P. Böhm, D. Sestak, D. Jares, V. Weinzettl, J. Stöckel, M. Hron, R. Panek, R. Scannell, and M. J. Walsh, "Progress of development of thomson scattering diagnostic system on compass)," *Review of Scientific Instruments*, vol. 81, no. 10, p. 10D531, 2010.

[18] S. C. McCool, I. L. McCool, R. D. Bengston, and P. E. Phillips, *Calibration of Thomson Scattering Density Measurements*. University of Texas, 1981.

[19] R. J. Groebner and T. N. Carlstrom, "Critical edge parameters for h-mode transition in diii-d," *Plasma Physics and Controlled Fusion*, vol. 40, no. 5, p. 673, 1998.

[20] M. A. Mahdavi, R. Maingi, R. J. Groebner, A. W. Leonard, T. H. Osborne, and G. Porter, "Physics of pedestal density profile formation and its impact on h-mode density limit in burning plasmas," *Physics of Plasmas (1994-present)*, vol. 10, no. 10, pp. 3984–3991, 2003.

[21] EXELIS Inc., *IDL documentation center*.

[22] E. Štefániková, P. Böhm, P. Bilkova, M. Aftanas, V. Weinzettl, J. Stöckel, M. Hron, and R. Panek, "Evolution of electron temperature and density profiles in edge transport barrier in the compass tokamak," in *Symposium on Plasma Physics and Technology*, June 2014.

[23] M. Aftanas, P. Bohm, P. Bilkova, V. Weinzettl, J. Zajac, F. Zacek, J. Stockel, M. Hron, R. Panek, R. Scannell, and M. J. Walsh, "High-resolution thomson scattering system on the compass tokamak: Evaluation of plasma parameters and error analysisa)," *Review of Scientific Instruments*, vol. 83, no. 10, p. 10E350, 2012.

[24] J. Ongena, I. Voitsekhovitch, M. Evrard, and D. McCune, "NUMERICAL TRANSPORT CODES," *Trans. Fusion Sci. Technol.*, vol. 57, pp. 381–390, 2010.